Development of an efficient nano-fluid cooling/ preheating system for PV-RO water desalination pilot plant

Development of an efficient nano-fluid cooling/preheating system for PV-RO water desalination pilot plant

S. M. Shalaby[a,*], M. K. Elfakharany[a,b], I.M. Mujtaba[b], B. M. Moharram[a], H. F. Abosheiasha[a]

[a]*Engineering Physics and Mathematics Department, Faculty of Engineering, Tanta University, Tanta 31733, Egypt*

[b] *Chemical Engineering Department, Faculty of Engineering & Informatics, University of Bradford, West Yorkshire BD7 1DP, UK*

Abstract:

In order to improve the performance of the reverse osmosis (RO) desalination plant powered by photovoltaic (PV), two cooling systems were proposed in this study to cool the PV and preheating the RO feed water as well. In the cooling design (1), the cooling fluid flows in direct contact with the back surface of the PV through channels of half circular cross-sections. While in the design (2), it flows through channels of squar cross-sections fixed on the PV back surface. Two nano-fluids were also tested as cooling fluid: H_2O/CuO and H_2O/Al_2O_3, in addition to distilled water for the purpose of comparison. The effect of changing the weight concentration of the nano-fluid (0.05, 0.1, and 0.15%) on the PV performance was also investigated. The results showed that the PV integrated with the cooling design (1) achieves better performance compared to design (2) at all studied cooling fluids. The improvements in the electric efficiency of the PV integrated with design (1) reached 39.5, 34.8 and 27.3 % when CuO and Al_2O_3 nano-fluids and distilled water were used as cooling fluid, respectively, compared to the uncooled PV. Based on the obtained experimental results, the PV integrated with design (1) was selected to power the RO with H_2O/CuO nano-fluid of weight concentration 0.15% and flow rate 0.15 kg/s being used as the coolant. The RO powered by the improved PV was tested at different salinities of brackish water when the preheating technique was implemented. The results showed that the proposed PV-RO desalination system produces 366 l/day when brackish water of salinity 3000 ppm was used.

*corresponding author:

Email addresses: saleh.shalaby@f-eng.tanta.edu.eg, (S.M. Shalaby), i.m.mujtaba@bradford.ac.uk, (I.M. Mujtaba), hatem_fouad@f-eng.tanta.edu.eg (H. F. Abosheiasha)

Keywords: Photovoltaic, reverse osmosis, desalination, nano-fluids, cooling, preheating

1. Introduction

One of the most difficulties confronting governments is the lack of drinkable water, particularly in distant and desert places where the power infrastructure is often unavailable. It is well understood that the desalination process needs a significant quantity of energy which is reflected in the high cost per cubic meter of desalinated water. This high cost is exacerbated in remote places where power grid connections are prohibitively expensive, and fossil fuel transportation costs are likewise prohibitively expensive. As a result, alternate energy sources suited for water desalination technologies must be sought in these places.

Many solar water desalination technologies were intensively investigated in Egypt, such as solar still [1], solar-powered humidification-dehumidification (HDH) [2], and reverse osmosis (RO) [3]. Among these technologies, RO powered by photovoltaic (PV) is widely used worldwide [4, 5]. A detailed review on PV-powered RO was introduced by Shalaby [5]. The review focuses on the innovative designs that led to enhance the productivity of the desalination plant. The results reveal that it is not economical to use PV with batteries to power RO plants due to its high capital and operating costs. Where the cost of fresh water production was found 7.8 €/m^3 [6] when batteryless-PV-RO was used compared to 8.3 €/m^3 [7] for a similar system was integrated with batteries.

The PV system is adapted to work without batteries to drive the RO by directly connecting the PV to the DC motor-driven pump [8] or via a supercapacitor as an electrical regulator [9]. The PV can be integrated with the displacement pump via a computerized variable DC/DC converter as introduced by Kelley and Dubowsky [10]. These several connections configurations succeed to provide the electrical power required to drive the RO for up to 6 hrs per day and achieve a low cost per cubic meter of freshwater compared with the system integrated with batteries [6, 7, 11].

Cooling the PV and preheating the RO feed water are considered the most techniques used for improving the PV-RO performance. Tonui and Tripanagnostopoulos [12] studied the PV when a conventional air channel was used for cooling. They presented also two designs of air channels: one with thin metal sheet and the other with fins. Their results showed an improvement in the electrical efficiency of the PV reaches 30% and 28% when fins and thin metal sheet were used, respectively, compared to the conventional air channel. Since the specific heat of liquids is higher than gases, it is preferable to use them as cooling fluid in the various cooling systems of photovoltaic cells. Gomaa et al. [13] found that the energy recovery per day for the water-based cooling system could reach 10.2 % compared to 7 % for the air-based cooling systems. Water-based cooling systems were studied by many researchers where different techniques were used to improve the PV electrical efficiency. For example, water sprinklers were used by Krauter [14] to cool the PV by providing a thin layer of water over the cell. The technique was successful in reducing the PV surface temperature to 22 ˚C and improving its efficiency by 10.3%. Odeh and Bahnih's [15] study also showed an improvement in the PV efficiency, reaching about 15% when the top surface of the PV was cooled by water trickling.

Similar results were obtained when impingement jet cooling device was used to cool the PV [16]. Significant improvements in the PV performance were also obtained by spraying water on its front [17] and both front and back [18] surfaces with superiority to the later technique.

The PV integrated with a solar reflector was tested by Mohsenzadeh and Hosseini [19] when water was used in a closed-loop, including a heat exchanger, to cool the back surface of the module. Their results showed that the temperature of the PV integrated with a reflector was decreased from 95 ˚C to 50 ˚C when the proposed cooling technique was implemented. Another active cooling system was developed by Prudhvi and Sai [20], where water was injected on a panel fixed on the PV back surface to transfer the heat to a buried underground heat exchanger. The efficiency of the PV is improved by 7.75 % when their cooling technique is implemented.

In addition to the use of purified water as a cooling fluid, water-based nano-fluid has been shown more effective in reducing the PV temperature. Water-based aluminum oxide and copper oxide nano-fluids were tested by Chandrasekar et al. [21] for cooling the PV. They tested those fluids with cotton wick in cooling the PV. Their system was dependent on using a cotton wick in a circular ring shape with 7 mm diameter and mounted to the PV backside. The cotton wick had free ends dipped in various fluids such as water, CuO/water nano-fluids, and Al_2O_3/water nano-fluids. Their results showed that the maximum powers of the cooled PV were 44.6 and 47.5 W when using a wick with nano-fluids and water, respectively, compared to 41 W for without cooling PV. The maximum PV efficiency was found to be 10.4 % when using a wick with water compared to 9 % without cooling PV. An empirical study was presented by Ghadiri et al. [22], where Fe_3O_4 water-based nano-fluid at two weight concentrations, 1 and 3%, were used for PV cooling. They studied the cooling effect on the thermal and electrical efficiency of the cell. Their results revealed that the system's overall efficiency was enhanced by 45 % when the nano-fluid of 3% weight

concentration was used. Ebaid et al. [23] presented a study about the effect of using nano-fluids aluminum oxide (Al_2O_3) and titanium oxide (TiO_2) with water-based nano-fluid at different concentrations. Their results showed that utilizing Al_2O_3 nano-fluid gave a higher enhancement in the efficiency of PV cells than TiO_2 nano-fluid.

Recently, with the increase in installing the PV-powered RO, many researches were done for preheating the RO feed water by using it as the cooling medium [10, 24]. Gorjian et al. [25] experimentally studied the PV-RO when the feed saline water was used as cooling medium. In this technique, the saline water is preheated by flowing through copper tubes fixed on the back surface of the PV before entering the RO. They concluded that the maximum productivity was obtained at circulating water temperature and salinity were 40 ˚C and 10000 ppm, respectively; while, less significant effect of feed water preheating on the RO productively was recorded at salinity 15000 ppm.

In another technique, Rezvan Talebnejad et al. [26] presented a study on improving the efficiency of the PV-RO system. To improve the efficiency of PV, increase RO productivity, and reduce the operating cost, they used the RO brine to cool the PV module. They also studied the effect of feed water preheating and salinity on the system productivity. The tests were carried out at different feed water temperatures (20, 25, 30, 35, and 40 ˚C) when water of total dissolved solids (TDS) of 1500, 3000, and 4500 mg L^{-1} were used. Their results showed that increasing the feed water temperature reduces the reject brine and increases the recovery factor. They also found that the maximum improvement in the electrical efficiency of the PV with cooling is 20 % compared to uncooled system.

The previous studies focused on studying the effect of changing the types, concentration, and flow rate of the nano-fluid used as cooling fluid on the performance of the PV. While the cooling

design system parameters such as heat transfer area, the shape of nano-fluid carrying channel, the thermal properties of the used material and its cost are out of scope in most of these studies. In addition, devolpement of PV integrated with a tight nano-fluid cooling system not only to drive the RO but also to preheat its feed water has not yet been implemented.

In this work, two advanced designs were tested for cooling the PV: in the first design, the cooling fluid flows in direct contact with the back surface of the PV through PVC channels of half circular cross-sections. While copper square channels fixed on the PV back surface were used for carrying the cooling fluid in the second design. The two cooling designs were tested when CuO and Al_2O_3 nano-fluids were used as heat transfer fluid (HTF). The HTF not only used as cooling medium but also for transferring the removed heat from the PV to RO feed water for preheating purpose. In the two cooling designs, the nano-fluid was circulated in a closed-loop through a nano-fluid tank, the cooling system, and a heat exchanger. So, very small amount of nanomaterial was used to prepare the nano-fluid. The cooling systems were also tested at different weight concentration of the nano-fluid. The PV integrated with the best cooling system, operated at the optimal operating conditions, was connected to DC motor-powered pump to drive the RO desalination plant. The effect of preheating the feed water and changing its salinity on the RO productivity was also studied.

2. Experimental work

The PV-RO experimental test rig was installed at the Faculty of Engineering roof, Tanta University, as shown in Fig. 1. All experiments were conducted during the summer of 2021. The conducted experiments aimed to improve the efficiency of the photovoltaic in order to efficiently operate the RO unit. Two cooling designs were installed and fixed on the back surfaces of two PV cells of 0.25 kW and simultaneously tested. In this section, the PV cooling systems design,

construction, material, operating parameters, and testing procedure are presented in detail. The proposed PV-RO configuration testing procedure is also introduced in this section.

2.1 PV Cooling system

The PV-RO system mainly consists of two components: the first is PV and the second is RO unit. Firstly, the cooling technique was used to improve the electric efficiency of the PV. The experimental test rig proposed for cooling the PV was included in the photograph shown in Fig. 1.

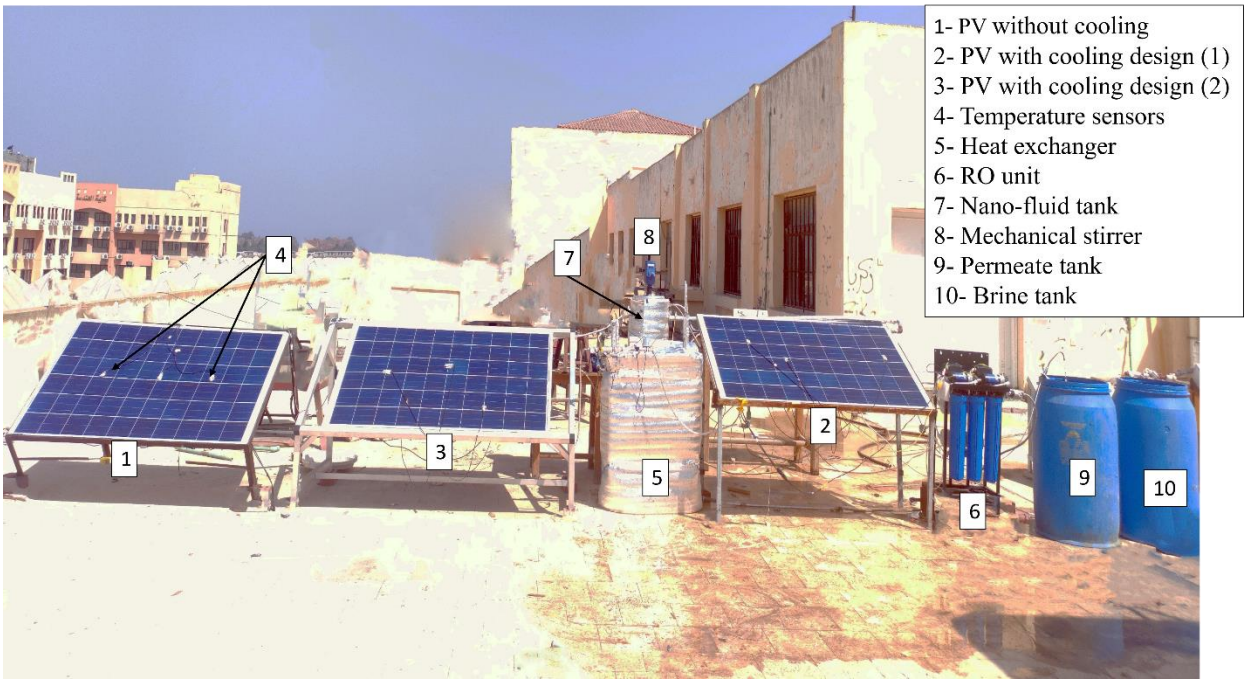

Fig. 1. Experimental test rig of the PV-RO integrated with two cooling/preheating design systems.

The system consists of three identical PV modules of rated power 0.25 kW, 37 V, 9 A, length and width 1.6, and 1.00 m, respectively. Each module was surrounded by an aluminum frame of a thickness of 3 cm.

In design (1), fifteen PVC tubes, of half-circular cross-sectional area, of 0.8 m length and 0.038 m diameter (1.5 inches) were directly fixed on the back surface of the PV module. The distance between each adjacent two tubes is 0.06 m. The header shown at the bottom was used to distribute the cooling fluid through the PVC tubes while the upper one was used to collect it as displayed in Fig. 2. This cooling system is very cheap and provides a direct contact between the cooling fluid and the PV surface.

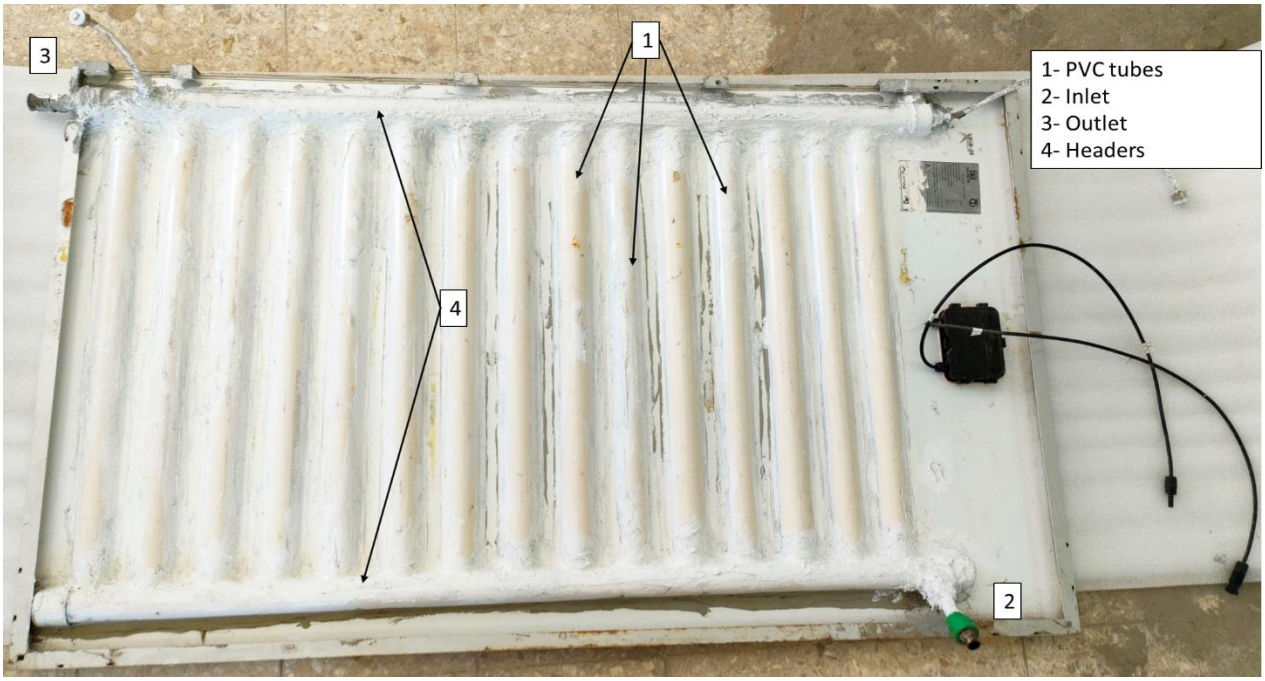

Fig. 2. Design (1) of the cooling system installed on the back surface of the PV module.

While in cooling design (2), eleven copper channels of square cross-sectional area, 2 cm × 2 cm, were connected in zigzag shape were used for carrying the cooling fluid as seen Fig. 3. The channel length is 1.30 m, and the space between each two adjacent channels is 0.06 m, as shown in Fig. 3. These channels were connected to a 1 mm copper plate using clamps and rivets. This plate was fixed at the back surface of the cell. In this design, channels of square cross sectional area were selected to increase the contacting area with the flat plate. The flat plate was also used to increase

the heat transfer between the PV back surface and the coolant. Channels made of copper were selected for carrying the cooling fluid due to the high thermal conductivity of copper despite of its high cost. For comparison, the reference PV module is tested free of cooling.

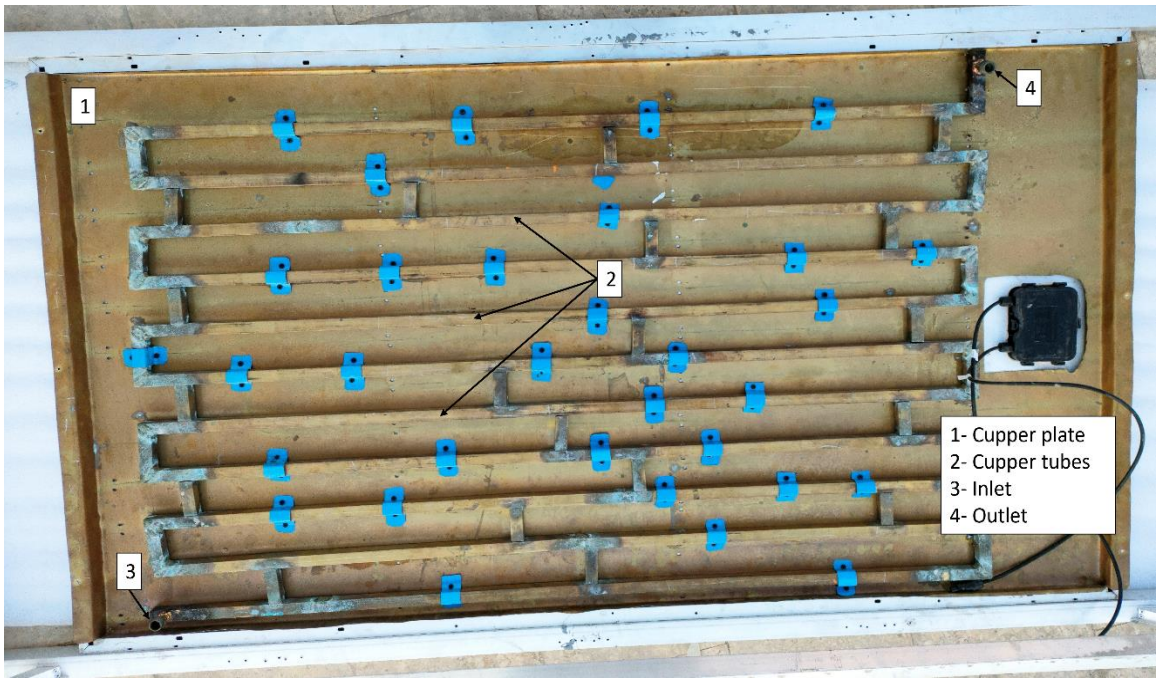

Fig. 3. Design (2) of the cooling system installed on the back surface of PV module.

In the case of nano-fluid was used for cooling, an electrical pump was used to circulate the nano-fluid through the cooling system and the nano-fluid tank of capacity 35 liters. A heat exchanger filled with water was also used to cool down the working fluid**.** The shell and finned tube heat exchanger was made of galvanized iron of internal length × width × height of 0.65×0.4×0.7 m. It was insulated with 5 cm thermal insulation, more detail about the shell and tubes heat exchanger can be found elsewhere [27].

2.2 PV-RO desalination plant

The PV integrated with the proposed cooling system is directly connected to DC motor-powered pump to drive the RO desalination system, as seen in Fig. 4. The RO unit with a capacity of 600

gallons of fresh water per day was used. The unit consists of four stages: the first stage is a polypropylene filter cartridge (PP cartridge filter) with a porosity of 5 microns. The second and the third stages are a carbon block pre-filter called "Chlorine, taste, and odor" (CTO) cartridge filter with a porosity of 10 microns. While the fourth stage is the RO stage which consists of two identical membranes with the technical characteristics shown in Table 1. The high-pressure pump used to drive the RO unit is a diaphragm booster pump with technical specifications summarized in Table 2.

Table 1. Technical characteristics of the membrane in RO unit

Model name	RE2812-300
Permeate flow rate GPD (L/day)	300 (1136)
Salt rejection %	97 %
Membrane type	Thin film composite
Membrane material	Polyamide (PA)
Element configuration	Spiral wound, tape wrapping
Membrane area	1.3 m^2
Membrane pore size	0.0001 μm

Table 2. Technical specification of the pump used in RO unit

Parameter	PUR-300G
Max. current	≤ 2.6 AMP
Max. pressure	140 PSI
Max. flow rate	≥ 3.5 LPM
Input voltage	24 VDC
Rated flow rate at 70 PSI	≥ 2.2 LPM
Rated current at 70 PSI	≤ 1.5 AMP

2.3 Experimental procedure

The PV integrated with the proposed cooling system was mainly studied to power the RO and preheat its feed water. The two designs were compared in terms of cooling efficiency when water and two types of nano-fluid were used as a cooling fluid. Two nanomaterials were used, namely

CuO and Al_2O_3, to form the nano-fluid using water as a base liquid. Three nano-fluids weight concentrations were prepared: 0.05 %, 0.10 %, and 0.15 %. A surfactant was also added for stabilizing the nanomaterials in water. Surfactants are chemical substances added to nanoparticles to reduce the surface tension of liquids and promote particle immersion. Large molecules, such as polymers and surfactants, adsorbed on the surface of particles in a stabilized dispersion inhibit re-agglomeration over time Nia et al. [28]. The Surfactant and nanomaterials were mixed with water by a mechanical stirrer.

An electrical pump was used to circulate the cooling fluid in a closed-loop, including a tank filled with 30 liters of nano-fluid, the cooling system, and a heat exchanger that was used to cool down the nano-fluid, as seen in Fig. 4.

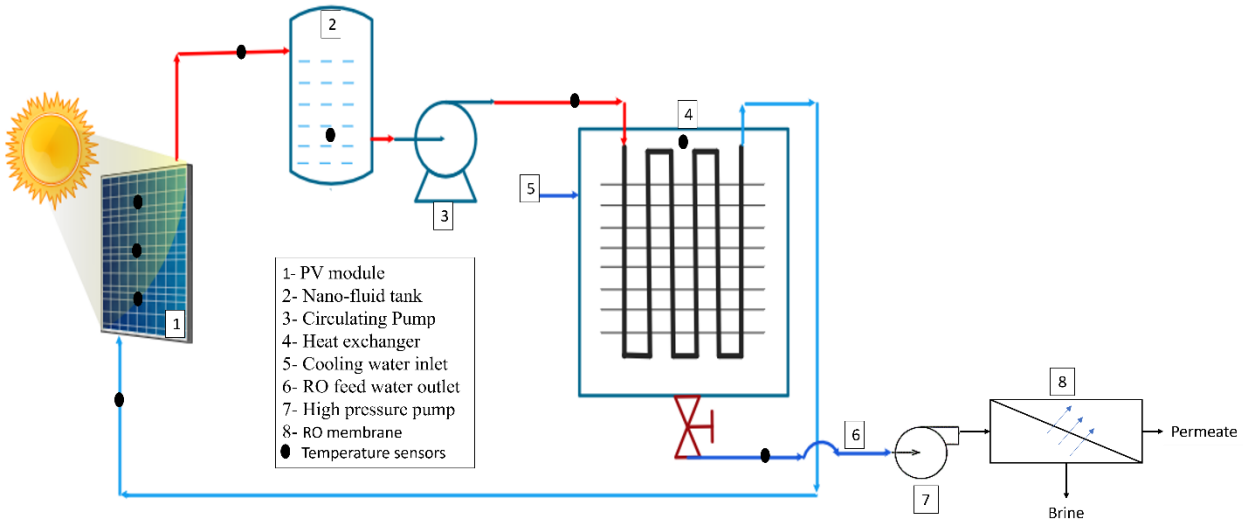

Fig. 4. Schematic diagram of the PV integrated with the cooling system and RO unit.

In order to optimize the flow rate of cooling fluid, the two cooling designs were firstly studied using distilled water as heat transfer fluid (HTF) at different mass flow rates ($\dot{m}_{HTF}$) (0.10, 0.15, and 0.21 kg/s. The discharging rate was controlled and measured by a ball valve and flow meter,

respectively. After that, the two designs were tested at the optimal flow rate of $\dot{m}_{HTF}$ when nano-fluids with several weight concentrations (0.05, 0.10, and 0.15 % (wt.)) were used as a cooling fluid. During testing the PV with all proposed cooling techniques, the PV free of cooling was also simultaneously tested. The current and the PV voltage were measured every hour at 14 different loads to estimate the PV generated power. Where maximum generated power P_{max} (W) was obtained as follows:

$$\boldsymbol{P_{max} = V_{opt} \times I_{opt}} \qquad (1)$$

Where $\boldsymbol{V_{opt}}$ (V) is optimum voltage, and $\boldsymbol{I_{opt}}$ (A) is the current at maximum power point.

The electrical efficiency of the PV ($\boldsymbol{\eta_{elec}}$) was also calculated:

$$\eta_{elec} = \frac{P_{max}}{P_{in}} \ . \qquad (2)$$

Where $\boldsymbol{P_{in}}$ is the incident power on the PV module which is calculated from the solar intensity as follows:

$$\boldsymbol{P_{in} = I \times A} \ . \qquad (3)$$

Where *I* is the solar intensity W/m^2, and A is the PV module area (m^2).

Finally, the PV with the selected cooling design was connected to DC motor-powered pump to drive the RO. The proposed PV-RO plant was also tested at different feed water salinity and two different temperatures. The RO permeate, and the percentage of its salts were also measured.

DS18B20-digital temperature sensors were used to measure the temperatures at different locations of the system. The used temperature sensor has accuracy of ± 0.5 ˚C and range -55 – 125 ˚C. The measured temperatures were recorded every 5 minutes using an Adriano microcontroller connected to a laptop. For example, for measuring the temperature of the PV front surface (T_{fs}), 3 temperature sensors were fixed at the top surface of the module then the average value was calculated. Similar technique were used to measure the back surface temperature (T_{bs}). The solar

radiation was measured from 9:00 am to 5:30 pm during all experiments using a High Precision Pyranometer (HPP) model MS-802. The HPP measures the global solar radiation with a sensitivity of 7.03 μv/W.m^2.

The permeate and the brine flow rate were also measured using an electronic flow meter (FS200A G $\frac{1}{2}^{"}$).

3. Results and discussion

This study proposed two PV cooling designs: the first, using PVC tubes, has a half-circular cross-section that provides a direct water contact with the PV back surface. The second uses copper tubes that have rectangular cross-section area.

For each studied case, the I_{opt} and V_{opt} were measured to determine the electric power and electrical efficiency for the PV module. The temperatures of front and back PV surfaces, cooling fluid inlet, outlet, and ambient were also measured. All measurements were conducted during the summer of 2021 at the Faculty of Engineering, Tanta University, Egypt.

3.1 Development of the PV cooling system

In this section, the results of optimizing the operating and design parameters that aim to improve the performance of PV cooling systems are presented. This includes optimizing the mass flow of the coolant fluid using distilled water as HTF. The two cooling configurations were also tested using distilled water/CuO nano-fluid and distilled water/Al_2O_3 nano-fluid. The effect of nano-fluid weight concentration is also presented in this section. Finally, the best configuration with optimal operating parameters is recommended to power the RO desalination plant.

3.1.1 Optimizing the mass flow rate of coolant fluid.

In the beginning, the experiments of cooling the PV using distilled water were conducted to determine the optimum $\dot{m}_{HTF}$ among the three proposed values. Over six days at approximately similar weather conditions, the experiments were conducted, the operating and weather parameters were measured, and the cell performance was estimated. During these experiments, the maximum measured values of solar radiation were found in the range between 959 and 980 W/m^2, while the daily average values of ambient temperature were found in the range 40.5-41.5 ˚C.

The effect of varying $\dot{m}_{HTF}$ on T_{fs} and T_{bs}, when the PV was tested using cooling design (1), are displayed in Fig. 5 and Fig. 6, respectively. It is clearly seen in these figures that a considerable drop in the PV surfaces temperatures was found when the cooling technique was implemented. This drop in the PV surfaces temperatures significantly increases with increasing the coolant flow rate from 0.1 to 0.15 kg/s, as plainly seen in Figs. 5 and 6. While the reduction in the PV surfaces temperatures is insignificant when the flow rate is increased from 0.15 to 0.21

kg/s. This is consistent with the results of Pang et al. [29] and Hossain et al. [30].

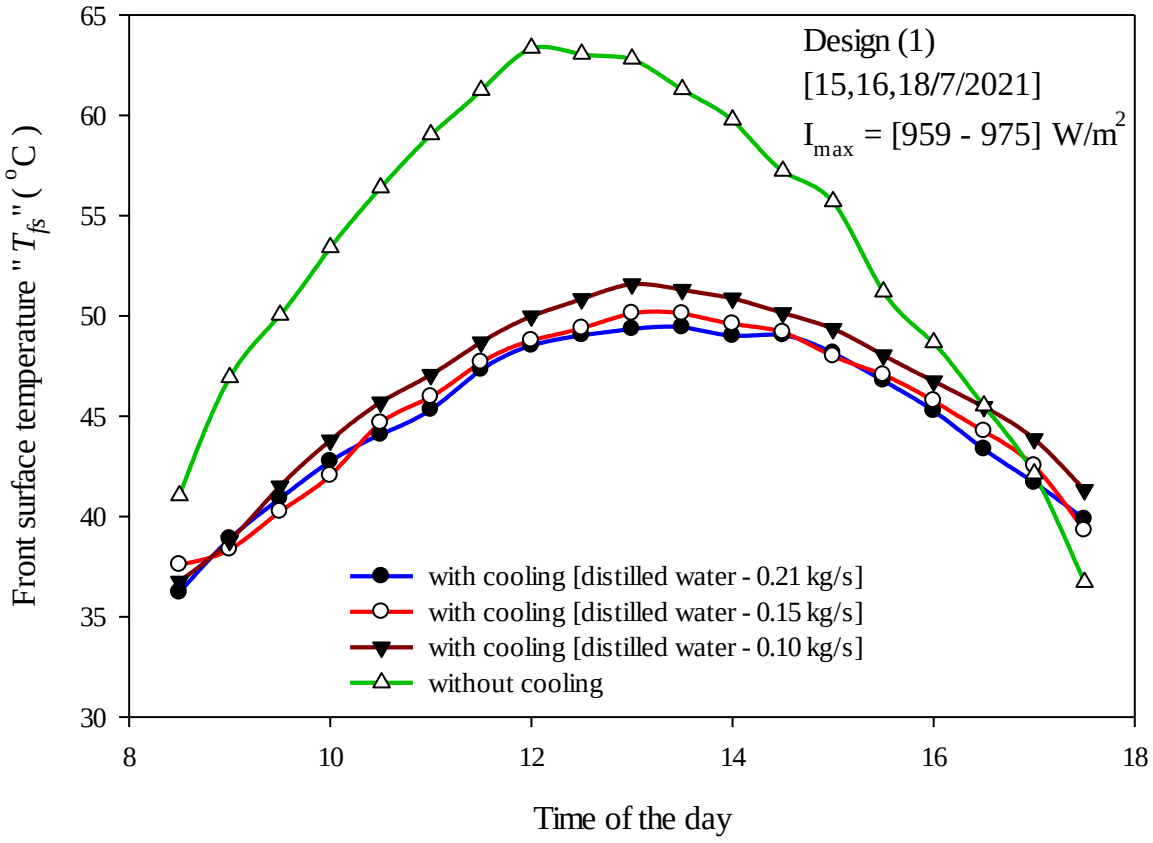

Fig. 5. The effect of mass flow rate on the front surface temperature when distilled water was used as cooling fluid.

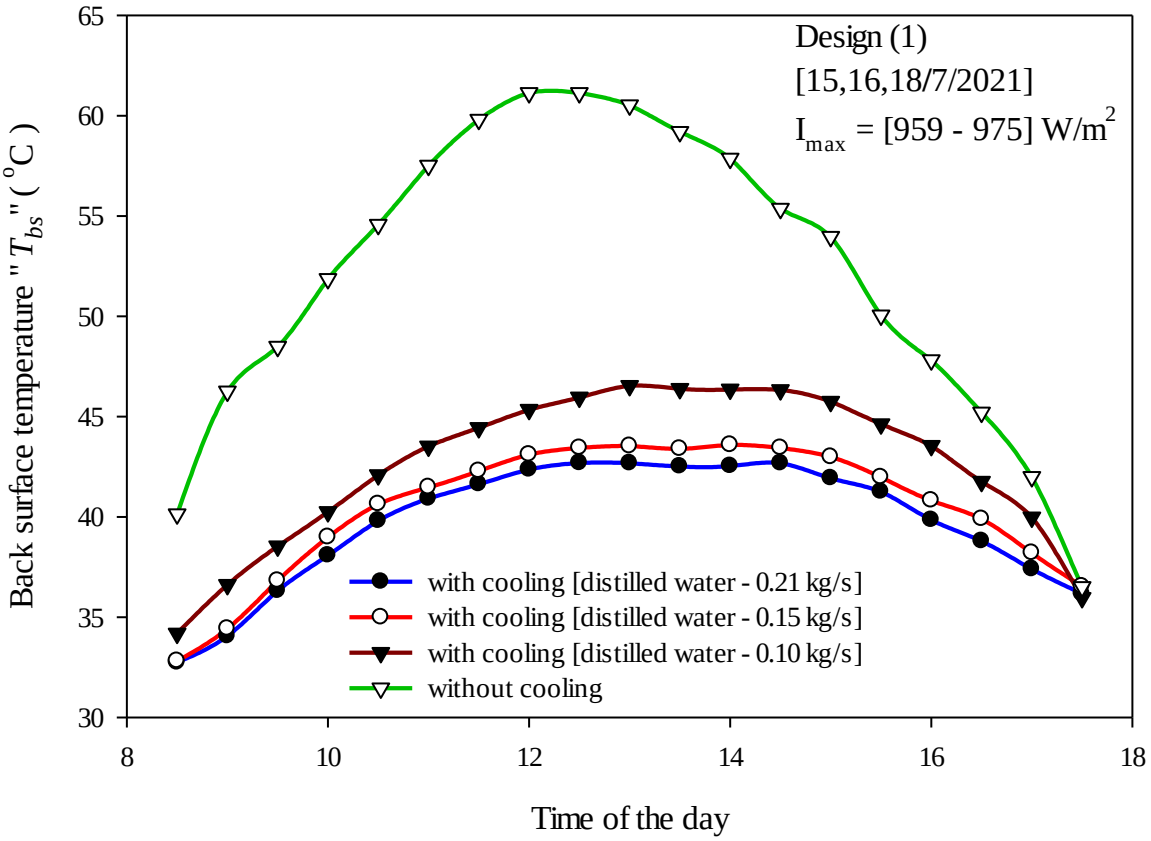

Fig. 6. The effect of mass flow rate on the back surface temperature when distilled water was used as cooling fluid.

The maximum measured values of T_{fs} and T_{bs} for the uncooled PV were 63.74 and 61.25 ˚C, respectively, compared to 49.5 and 43.1 ˚C for the cooled PV when $\dot{m}_{HTF}$= 0.15 kg/s was used. This means that the drop in T_{fs} and T_{bs} was found in the range 5 -14 ˚C and 7-17.8 ˚C, respectively, compared to the system free of cooling. Approximately similar decrements in T_{fs} and T_{bs} reach 4 -14.1 ˚C and 6-18 ˚C, respectively, were found when $\dot{m}_{HTF}$= 0.21 kg/s was used.

It is also noticed that when the sun begins to fade, there is no need to cool the PV as the temperatures of the uncooled PV surfaces drop to lower values and become similar to that measured for the cooled system at sunset.

Similar results were found when design (2) were tested, where $\dot{m}_{HTF}$= 0.15 kg/s was found the optimal flow rate as it achieves a significant drop in T_{fs} and T_{bs} reach 8.2 ˚C and 11.5 ˚C, respectively, as seen in Fig. 7.

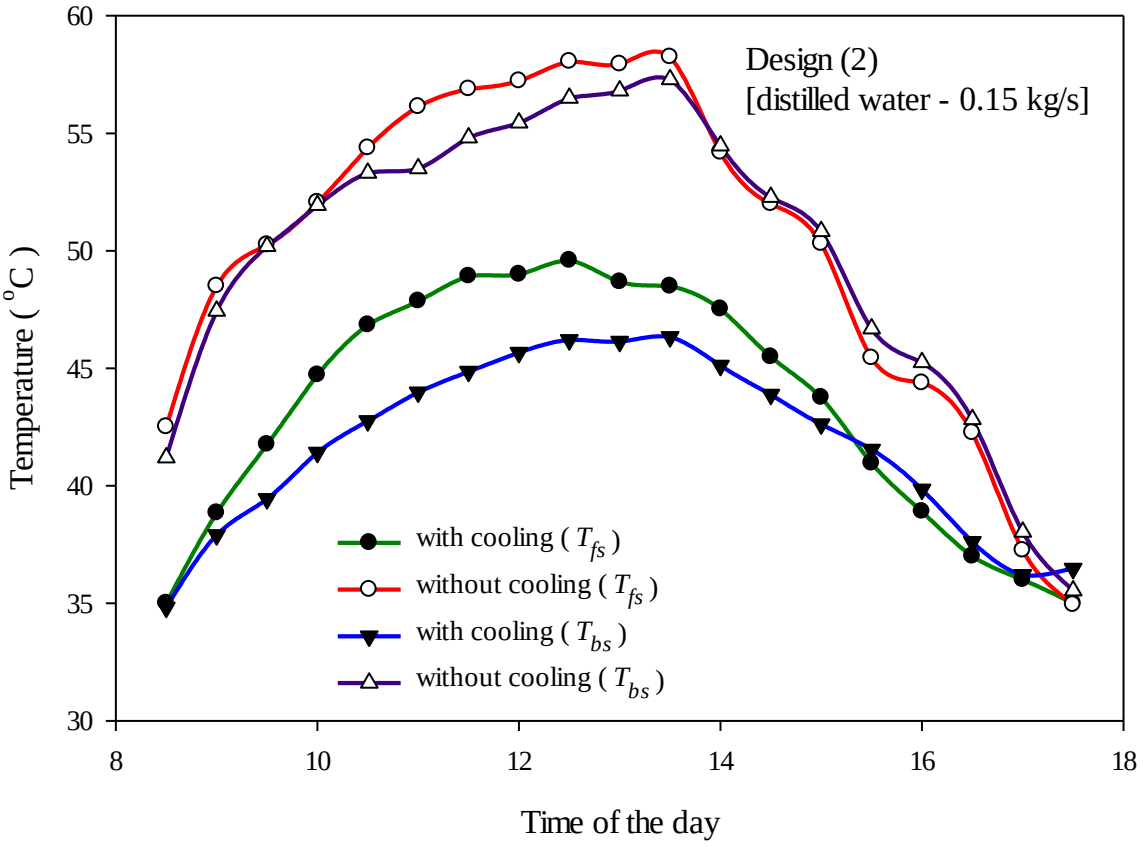

Fig. 7. The variation of T_{fs} and T_{bs} when distilled water was used as cooling fluid in design (2) at $\dot{m}_{HTF}$= 0.15 kg/s.

Cooling the PV has a positive effect on the PV surfaces temperature, as previously discussed. This positive effect was reflected in a significant enhancement on the electrical power and efficiencies for the both designs, as shown in Figs. 8-11. As can be clearly seen in Fig. Figs. 8 and 9, the PV optimal daily performance was achieved when the flow rate of 0.15 kg/s was used. A maximum power of 162.4 W is achieved, at this flow rate, compared to 126.4 W for the uncooled PV as

obtained from Fig. 8. So, the power generation of the PV integrated with cooling design (1) is improved by 28.5 % when $\dot{m}_{HTF}$= 0.15 kg/s was used. The displayed results in Fig. 8 also showed that a considerable power, more than 125 W, was generated during the period 9:00 am- 3:00 pm when $\dot{m}_{HTF}$= 0.15 kg/s was used. So, the PV integrated with design (1) can be operated for 6 hrs/day to drive a DC load of 125 W.

Figure 9 represents the variation of electric efficiency of the cooled PV over the day at the different used flow rate. The electrical efficiency of the water-cooled PV module was improved and achieved the best of performance at a flow rate of 0.15 kg/s, as plainly shown in Fig. 9.

Considering the period from 10:00 am to 5:00 pm, the maximum electric efficiency, maximum increment in electric efficiency, and the daily average increment in electric efficiency were found at 11.46 %, 29.29 %, and 26.97 %, respectively. High values of electrical efficiencies were recorded in the early morning (9:00 am) reaching 18.55, 18.44, and 17.06% when the coolant flow rate were 0.21, 0.15, 0.10 kg/s, respectively, compared to 13.86 % for the uncooled PV. The corresponding values recorded at noon were found to be 11.3, 11.46, and 10.93 %, respectively, compared to 8.86 % for the system without cooling. The low ambient temperature recoded at 9:00 am (32˚C) helped the cooling system, operated at the optimal conditions, to maintain T_{fs} and T_{bs} lower than 38.3 and 34.4 ˚C, respectively, as can be seen in Fig. 6. Therefore, high efficiencies were obtained in the early morning. The maximum drop in T_{fs} and T_{bs} recorded at noon that reaches14 and 18 ˚C respectively, is still insufficient to achieve high efficiency compared to that recorded at 9:00 am. So, the cooling system still needs more improvement. Based on the previous results, another design was proposed, and the two types of nano-fluid were also used as a coolant fluid.

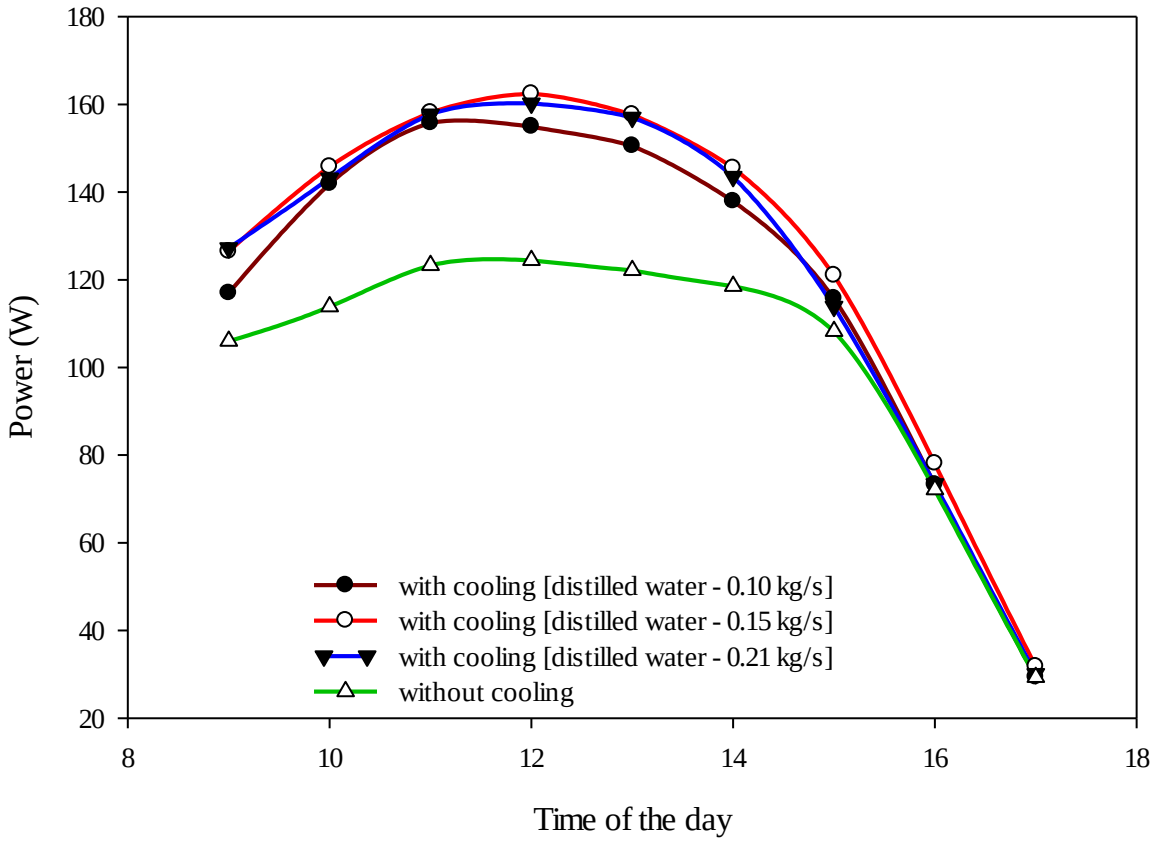

Fig. 8. The effect of changing the flow rate on the PV generated power when design (1) was used.

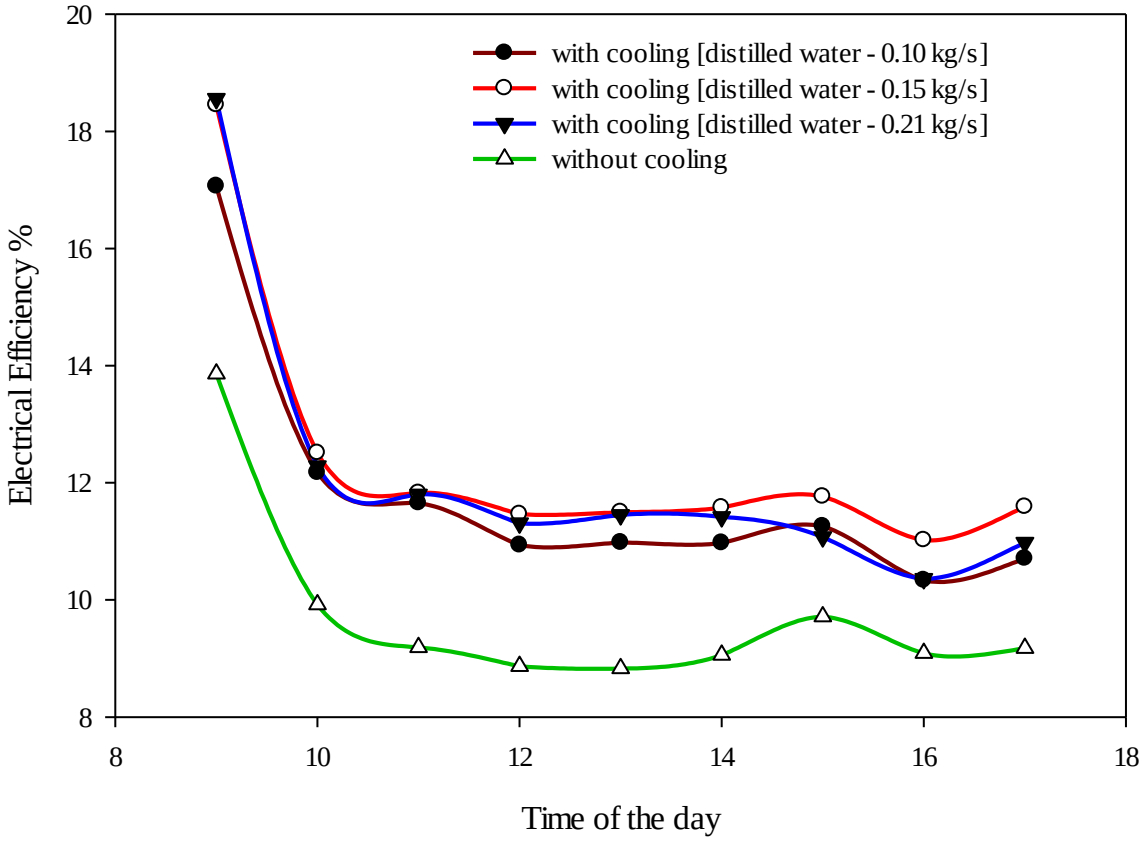

Fig. 9. The effect of changing the flow rate on the PV electrical efficiency when design (1) was used.

Figure 10 displays the PV power generation when cooling design (2) was used. It is observed that at a flow rate of 0.15 kg/s, the optimum value of the generated power of 159.976 W is obtained compared to 132.67 W for the uncooled PV. So, at this flow rate, the power generation of the cooled PV was improved by about 21 % when the proposed cooling design (2) was implemented.

The PV electrical efficiency is significantly improved when the cooling technique is implemented at all flow rates of HTF with little bet superiority at 0.15 kg/s as clearly seen in Figure 11.

In comparison to design (1), similar results were also obtained regarding the electrical efficiency improvement in the morning and at noon. Where maximum electrical efficiency recorded at noon were found 11.2 %, respectively, compared to 17.6% recorded at 9:00.am. So, the two cooling designs are still need more improvements. Based on the previous results, two types of nano-fluids were tested as coolant fluid within the two designs. These results are also convenient with [31] and better than the results obtained by [29, 30], whose electrical efficiencies recorded at noon are 10.5 and 10.4 %, respectively. The values of electrical efficiencies recorded at noon are considered much higher than the results reported by [32, 33] which are 6.9 and 9.9%, respectively.

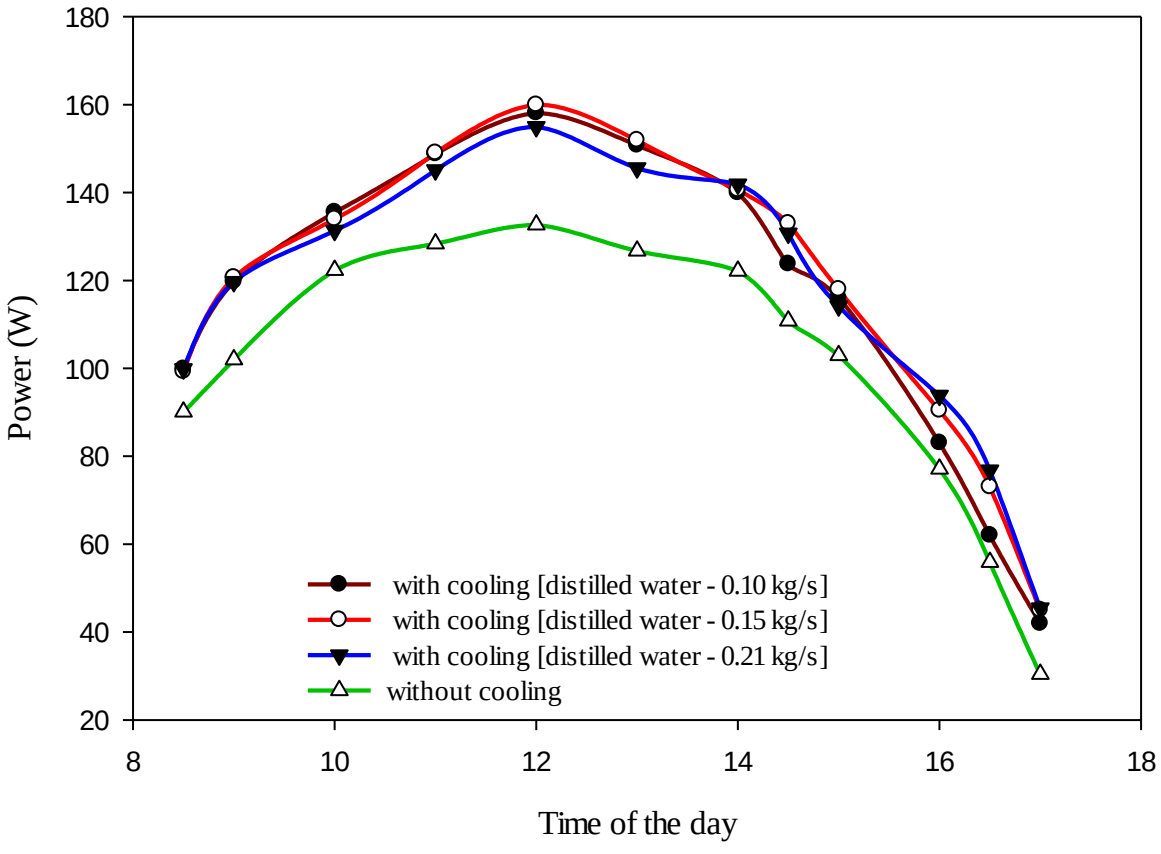

Fig. 10. The effect of changing the flow rate on the PV generated power when design (2) is used.

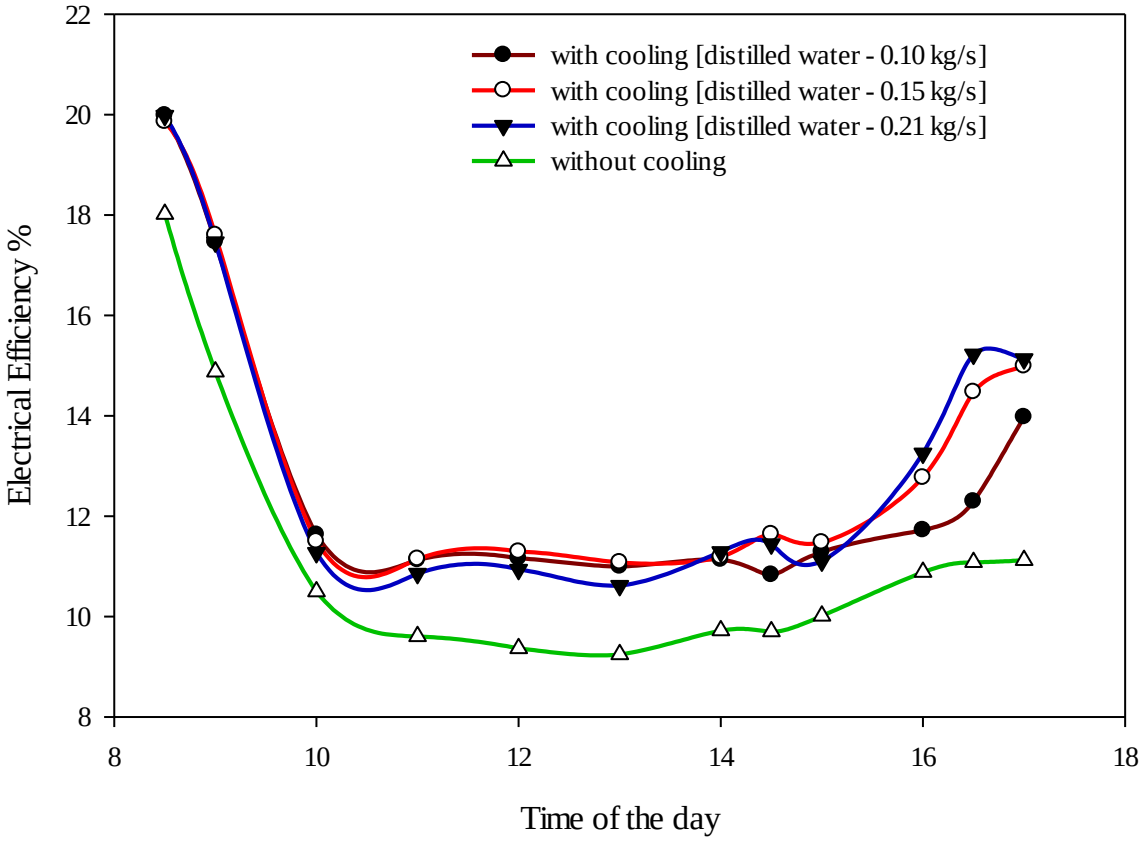

Fig. 11. The effect of changing the flow rate on the PV electrical efficiency when design (2) was used.

For both cooling designs, the previous results showed that the optimal performance of the PV was achieved when $\dot{m}_{HTF}$= 0.15 kg/s was used and where the best electrical power and efficiency were obtained. So, $\dot{m}_{HTF}$= 0.15 kg/s is the optimal flow rate; therefore, it will be considered while studying the effect of using nano-fluid with different concentrations as a coolant fluid.

3.1.2 The effect of using nano-fluid with different concentrations as a heat transfer fluid

In this study, two nano-fluids were tested as HTF: CuO and Al_2O_3 with distilled water as a base fluid.

3.1.2.1 Using H_2O/ CuO nano-fluid

The PV integrated with cooling design (1) was tested when H_2O/CuO nano-fluid was used as cooling fluid at the optimal HTF flow rate ($\dot{m}_{HTF}$= 0.15kg/s). The effect of cooling the PV on T_{fs} and T_{bs} are illustrated in Fig. 12 and Fig. 13 at three nano-fluid weight concentrations (0.05, 0.10, and 0.15 %). It is clearly seen in Figs. 12 and 13 that the best cooling performance was achieved when the highest weight concentration was used (0.15%). Reductions in T_{fs} and T_{bs} of 16.26 and 21 ˚C respectively were achieved compared to the system without cooling.

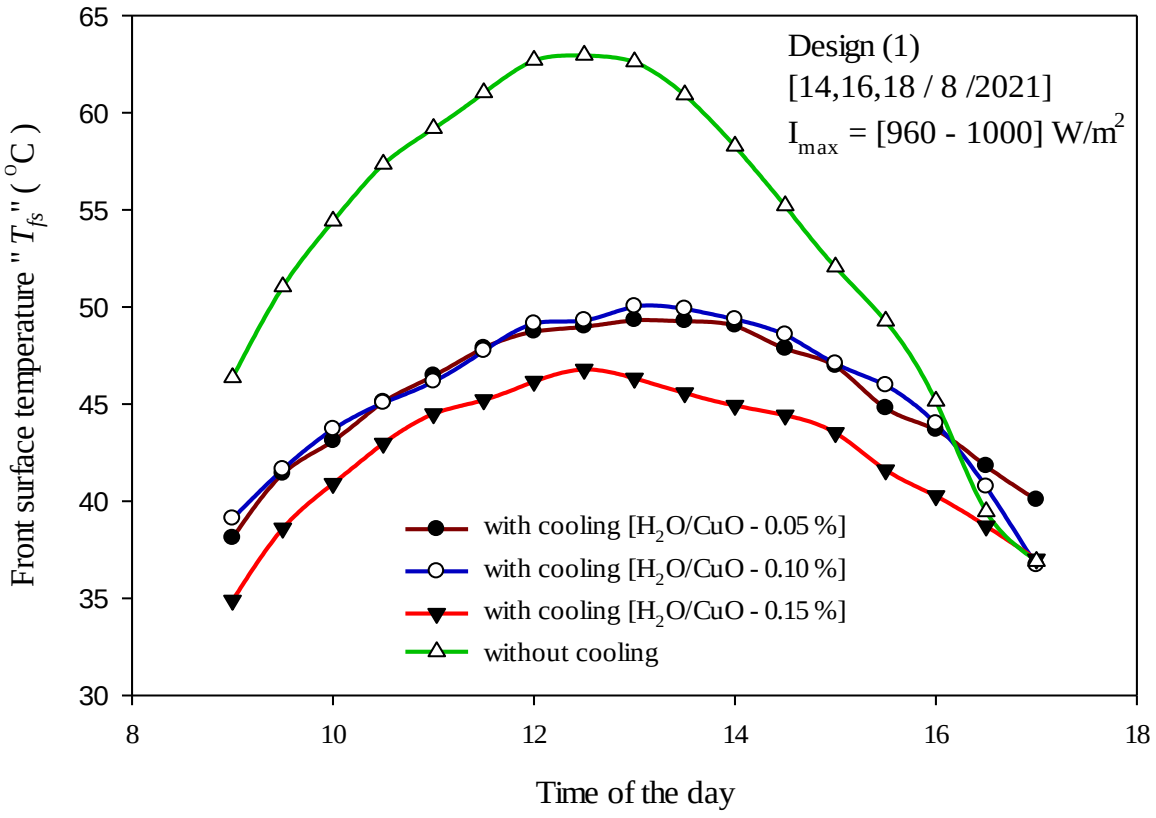

Fig. 12. The effect of changing the concentration of H_2O/CuO nano-fluid on the front surface temperature when design (1) was used.

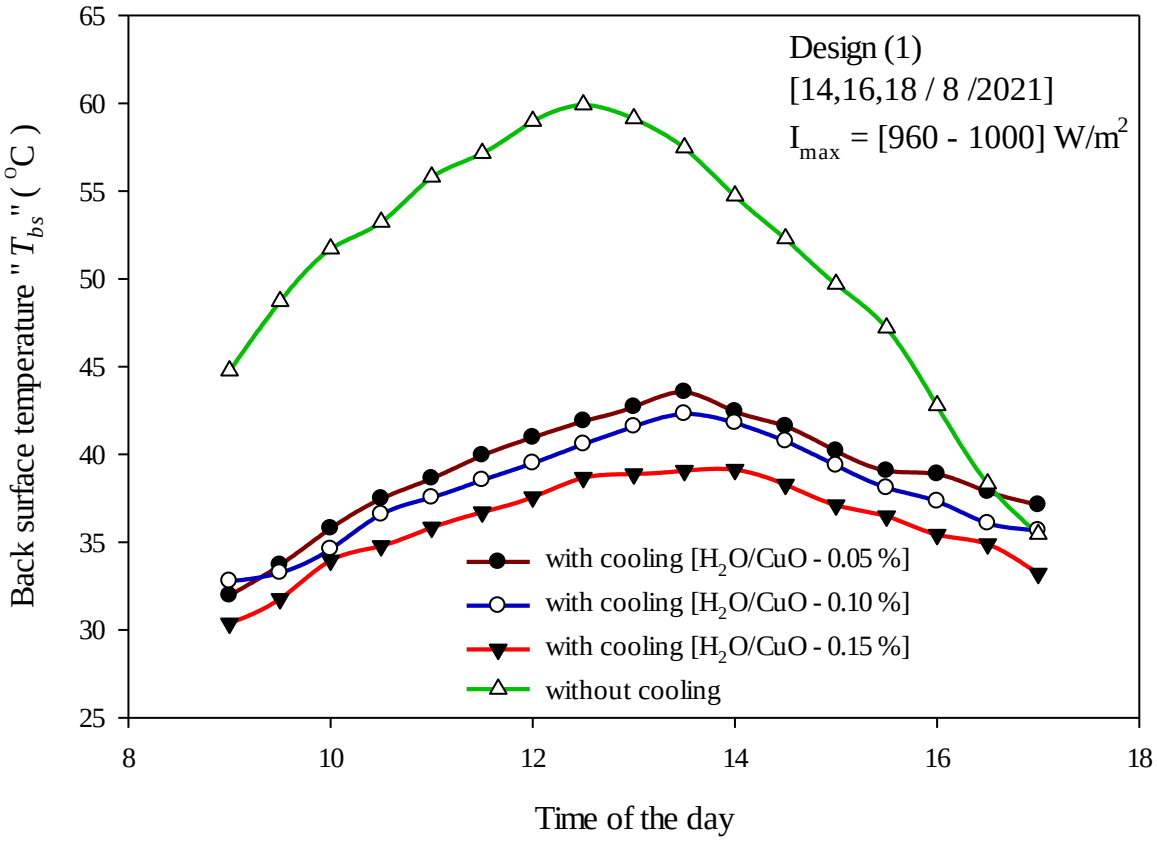

Fig. 13. The effect of changing the concentration of H_2O/CuO nano-fluid on the back surface temperature when design (1) was used.

Figure 14 displays the power generated from the PV integrated with design (1) at different values of CuO nano-fluid concentrations. Figure 14 shows that the best weight concentration of H_2O/CuO nano-fluid is 15 %, as it achieves the maximum power of 178.1W compared to 127.6 W obtained using the uncooled PV. This means that the PV generated power is improved by 39.58 % when the proposed cooling system was implemented. Accordingly, the best electrical efficiencies of H_2O/CuO nano-fluid-cooled PV at the highest nano-fluid concentration as visibly seen in Fig. 15, where the variations of electrical efficiencies of the cooled PV over the day are presented.

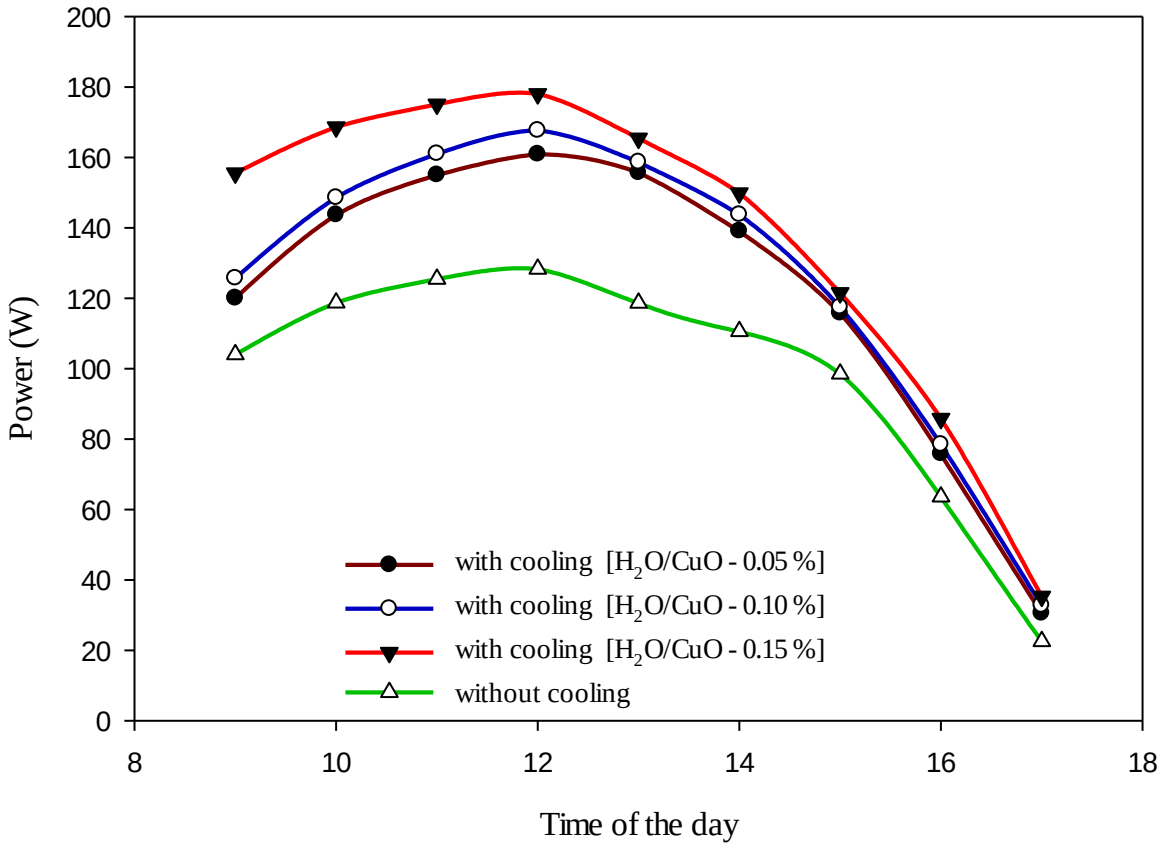

Fig. 14. The effect of changing the weight concentration of H_2O/CuO nano-fluid on the PV generated power when design (1) was used.

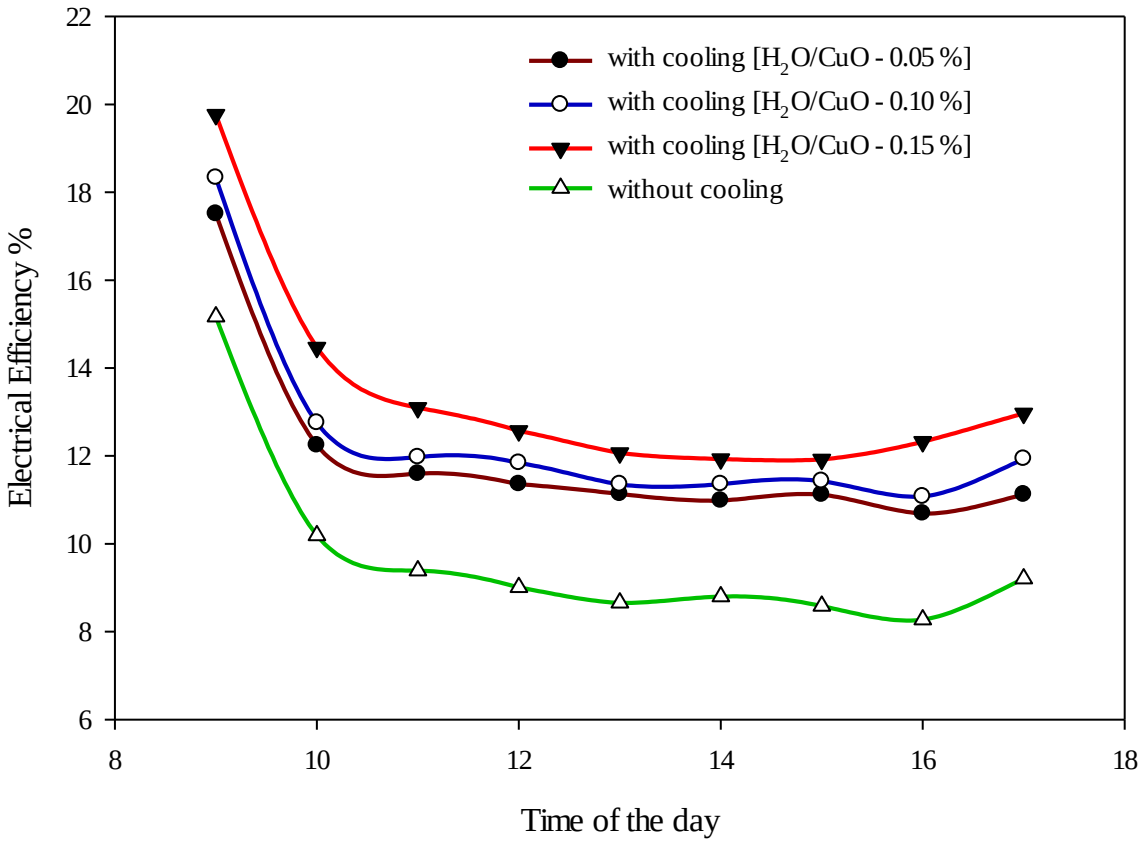

Fig. 15. The electrical efficiency of the PV at the different studied concentrations of H_2O/CuO nano-fluid when design (1) was used.

In the cooling design (2), the best cooling performance was also achieved at the highest nano-fluid concentration (15%), as displayed in Fig. 16 and Fig. 17. The maximum measured values of T_{fs} and T_{bs} are decreased from 59 and 55.7 ˚C to 48.96 and 40.48 ˚C when nano-fluid of weight concentration 15% is used. It also achieved drop-in T_{fs} and T_{bs} of 10 ˚C and 14.87 ˚C compared to the system without cooling.

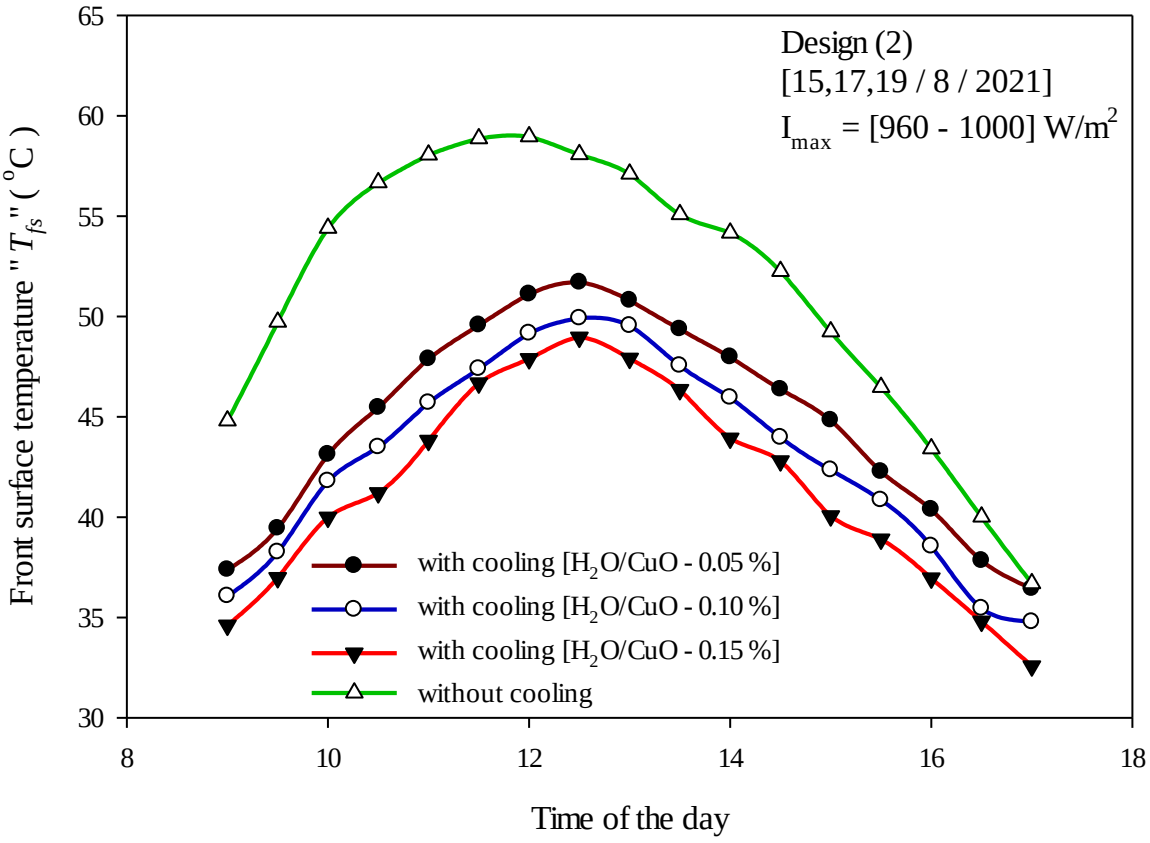

Fig. 16. The effect of changing the concentration of H_2O/CuO nano-fluid on the PV front surface temperature when design (2) was used.

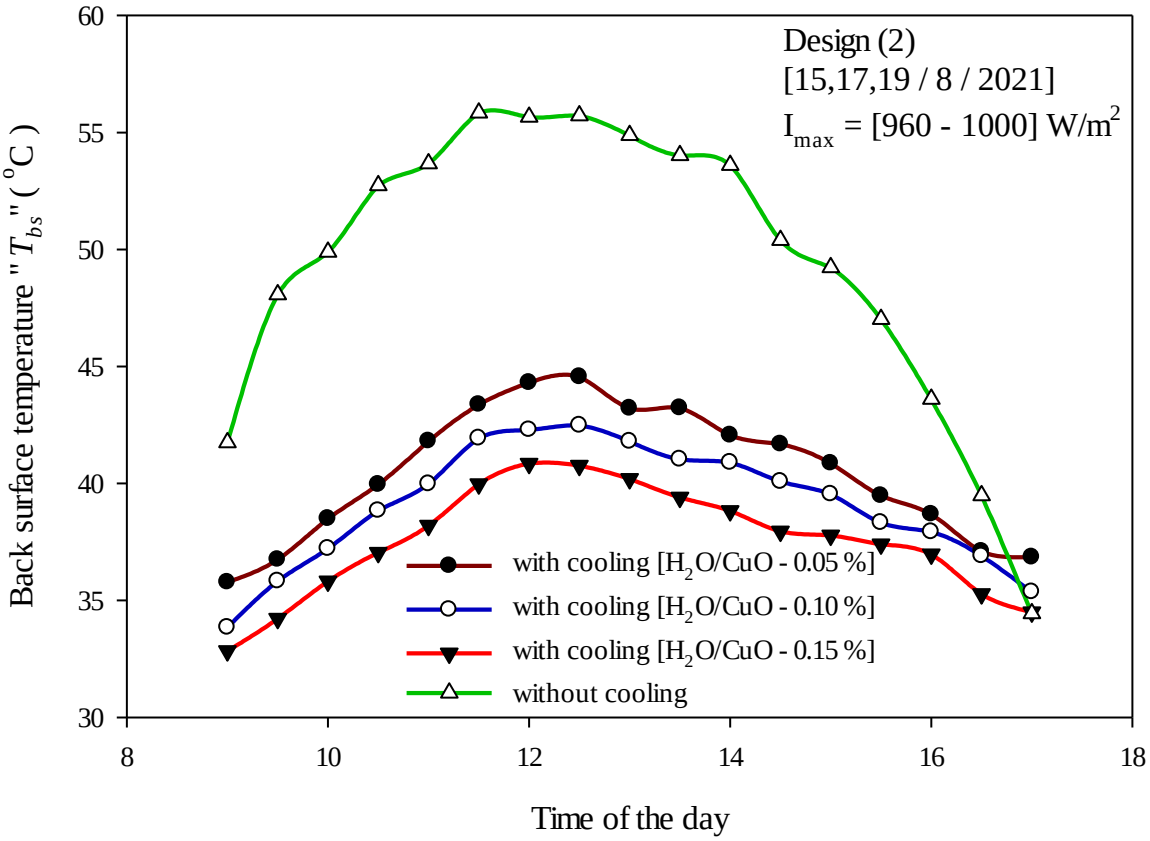

Fig. 17. The effect of changing the concentration of H_2O/CuO nano-fluid on the PV back surface temperature when design (2) was used.

3.1.2.2 Using Aluminum oxide (H_2O/Al_2O_3)

In the cooling design (1), the effect of cooling the PV was also studied when H_2O/Al_2O_3 was used as a cooling fluid. The effect of cooling the PV back surface on T_{fs} , T_{bs} are displayed in Fig. 18 and 19 at the different weight concentrations (0.05, 0.10, and 0.15 %).

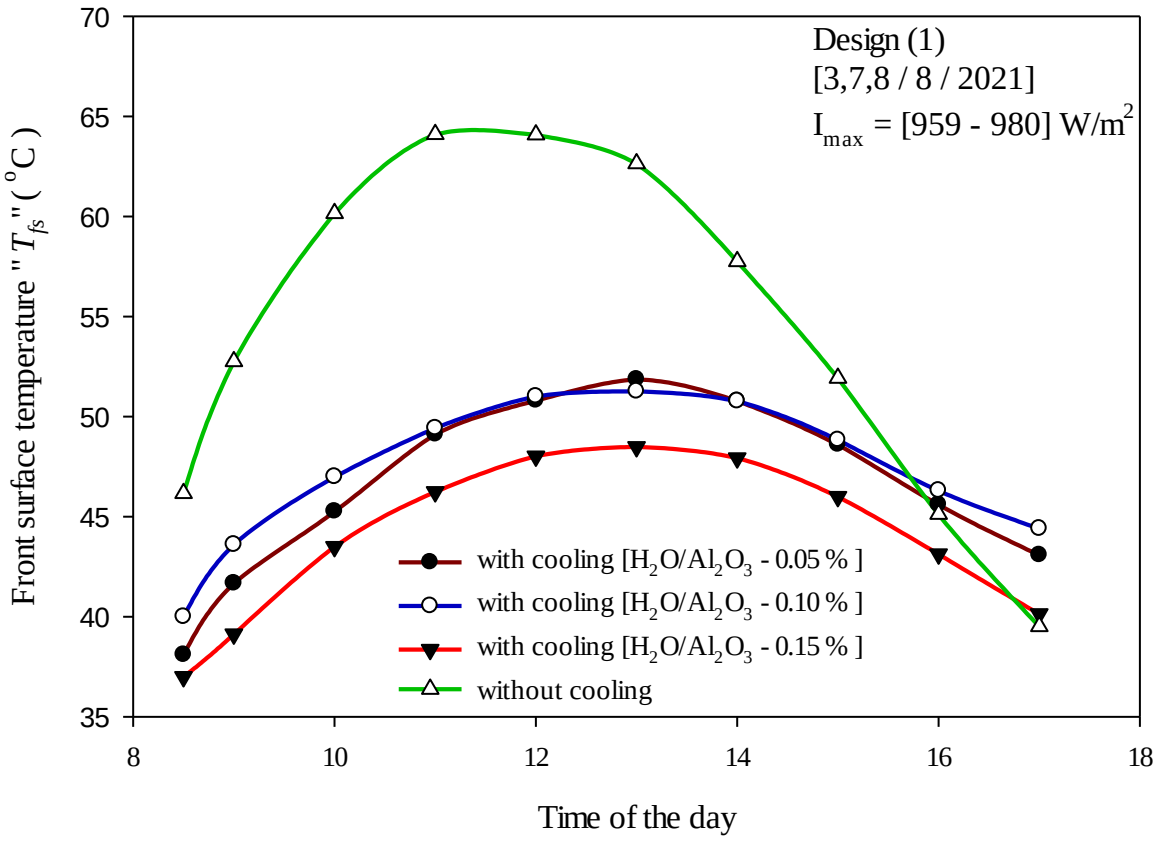

Fig. 18. The effect of changing the concentration of H_2O /Al_2O_3 nano-fluid on the front surface temperature when design (1) was used.

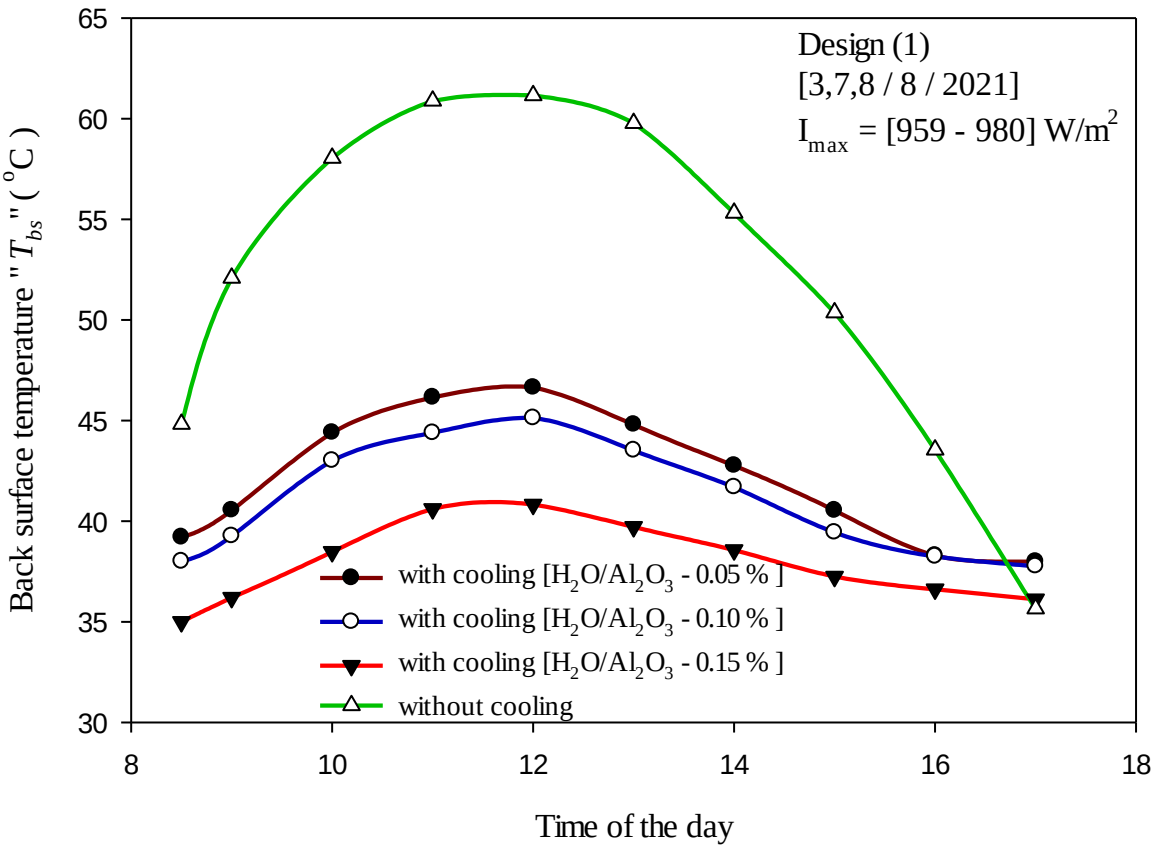

Fig. 19. The effect of changing the concentration of H_2O /Al_2O_3 nano-fluid on the back surface temperature when design (1) was used.

From the results illustrated in Figs. 18 and 19, the maximum drop-in T_{fs} and T_{bs} were achieved when the concentration of H_2O/AL_2O_3 nano-fluid was 15%. The drop-in T_{fs} was found to be 15.5 ˚C compared to 20.2 ˚C for T_{bs}. The peak values of T_{fs} and T_{bs} were also decreased from 64.1 and 61 ˚C to 48.48 and 40.82 ˚C, respectively, when H_2O/AL_2O_3 nano-fluid of 15% weight concentration was used. Similar results were also found for design (2) when H_2O/AL_2O_3 nano-fluid was used as a coolant fluid. The best cooling performance was also obtained at concentration 15%, as can be seen in Fig. 20 and 21. In the following sections, a comparison between the two nano-fluids is conducted at optimal flow rate and weight concentration for each design. This is

followed by comparing the two designs at the optimal operating conditions: best nano-fluid, HTF flow rate, and nano-fluid concentration.

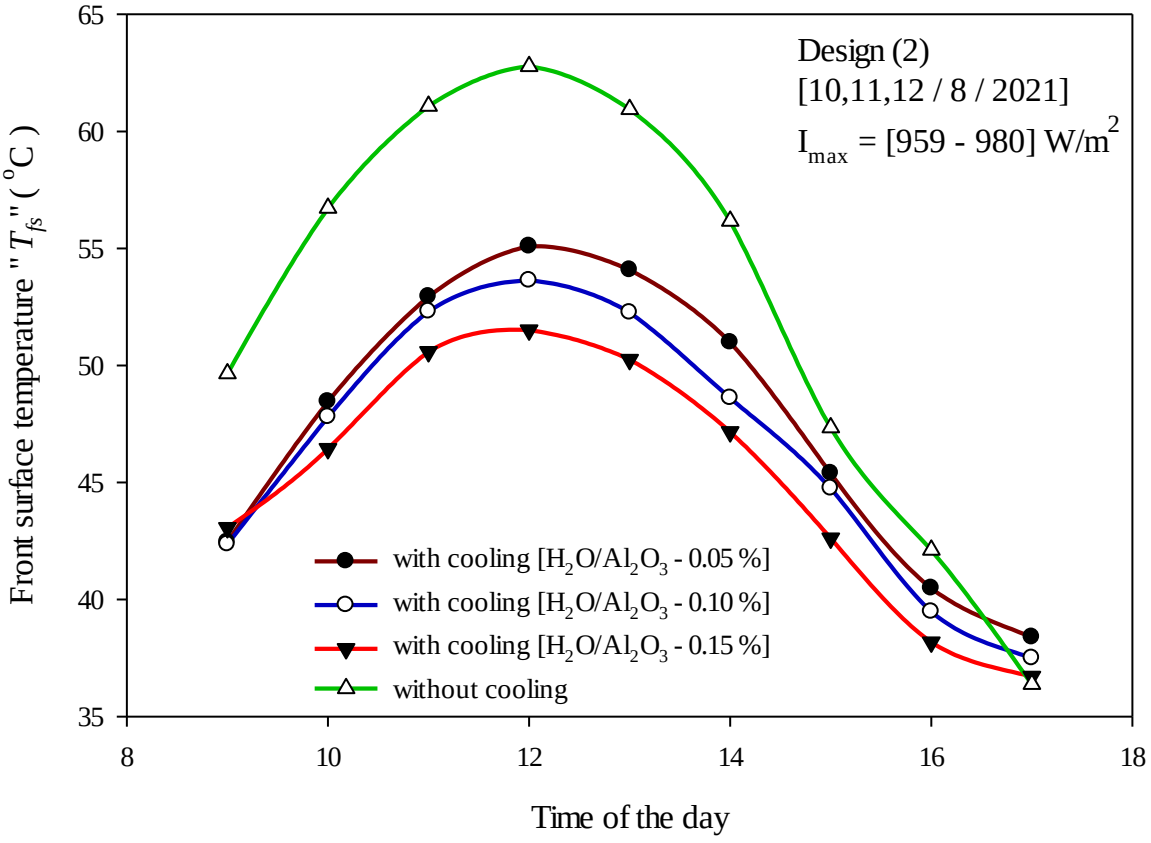

Fig. 20. The effect of changing the concentration of H_2O /Al_2O_3 nano-fluid on the front surface temperature when design (2) was used.

.

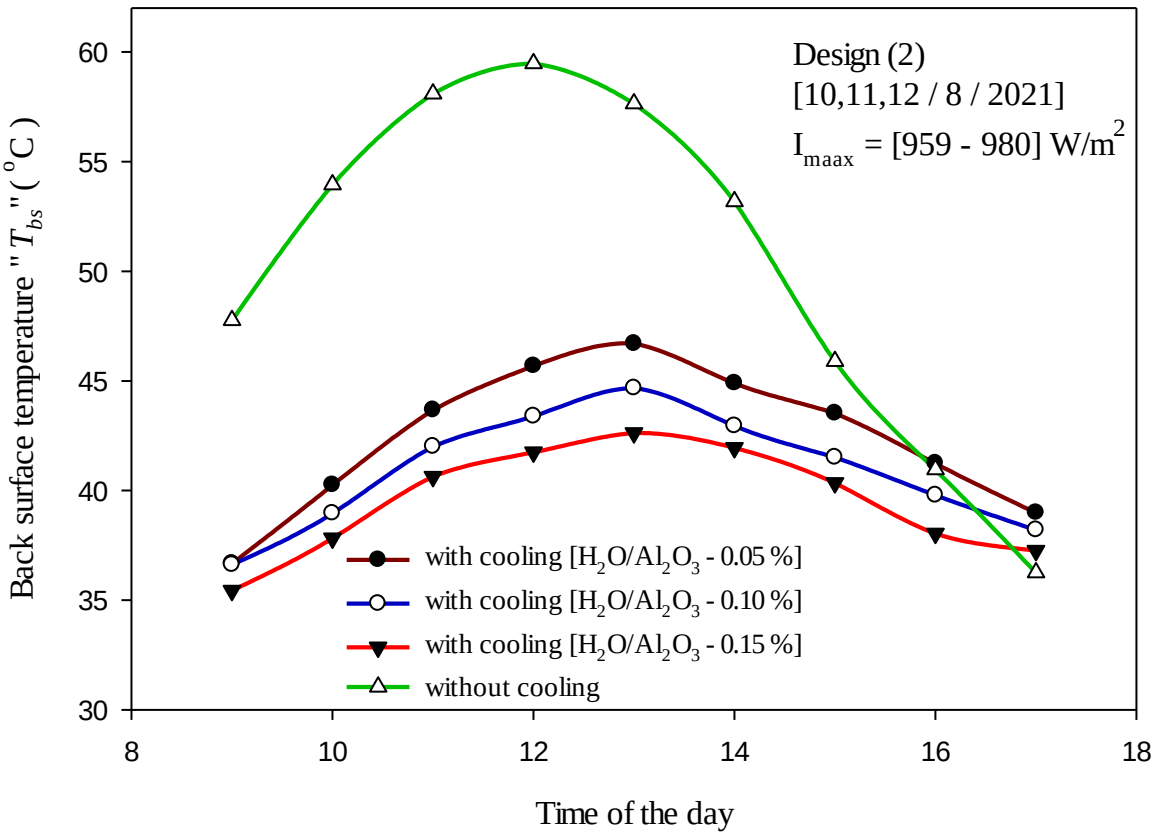

Fig. 21. The effect of changing the concentration of H_2O /Al_2O_3 nano-fluid on the back surface temperature when design (2) was used.

3.1.2.3 Comparison between H_2O/CuO and H_2O/Al_2O_3 as cooling nano-fluids.

Comparison between the power generated from the PV for different coolant fluids is displayed in Figs. 22 and 23 when the cooling design (1) and (2) were tested at the optimal flow rate and weight concentration of nano-fluid. In the two cooling designs, whatever the cooling fluid was, more generated power was obtained compared to uncooled PV, as can be seen in Figs. 21 and 22. The best performance of the PV was obtained when H_2O/CuO nano-fluid was used as coolant fluid, followed by Al_2O_3 nano-fluid then distilled water. From the results of cooling design (1) displayed in Fig. 22, the maximum generated power was 178.1 W when CuO nano-fluid was used compared to 172.04 W and 162.445 W for Al_2O_3 nano-fluid and distilled water, respectively. The maximum powers generation in design (2) were 162.871, 159.4, and 155.176 W when CuO, Al_2O_3 nano-fluids, and distilled water were used, respectively, as obtained from Fig. 23.

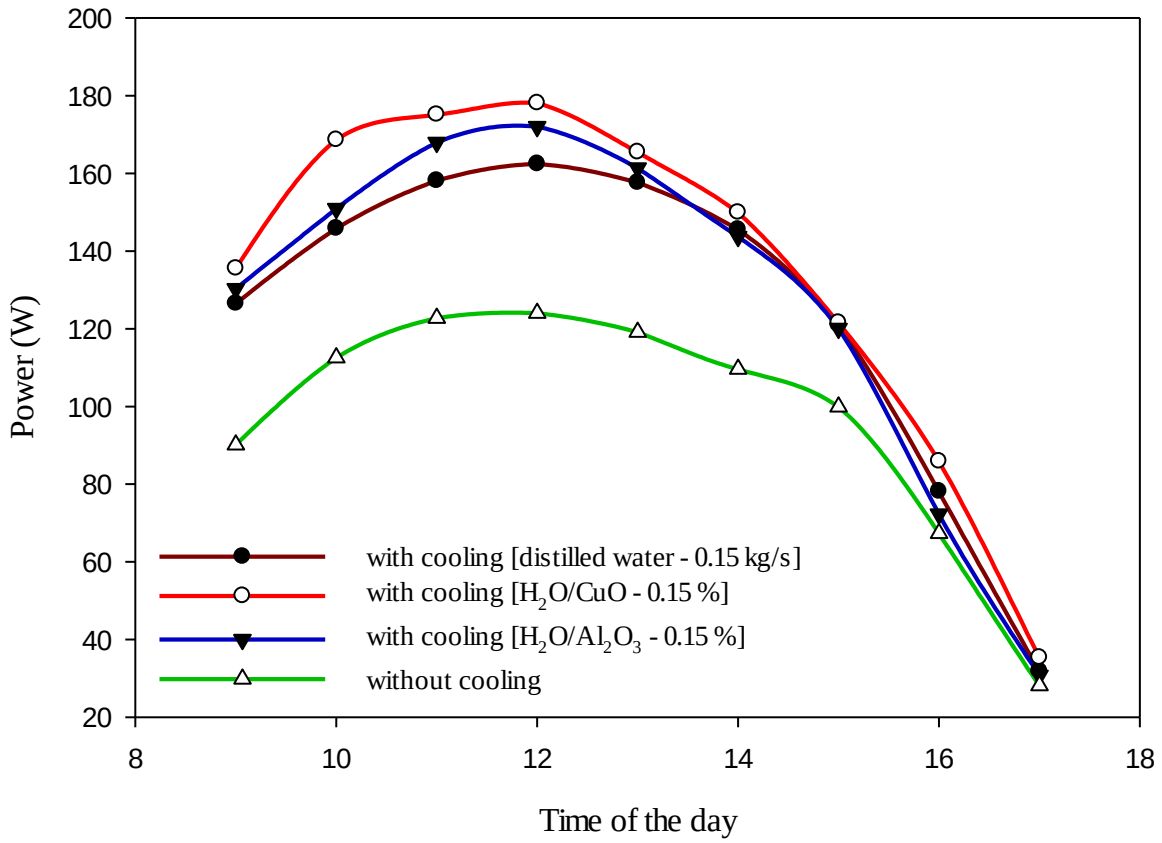

Fig. 22. Comparison between the power generated from the PV for different cooling fluids when design (1) was tested at optimal operating conditions.

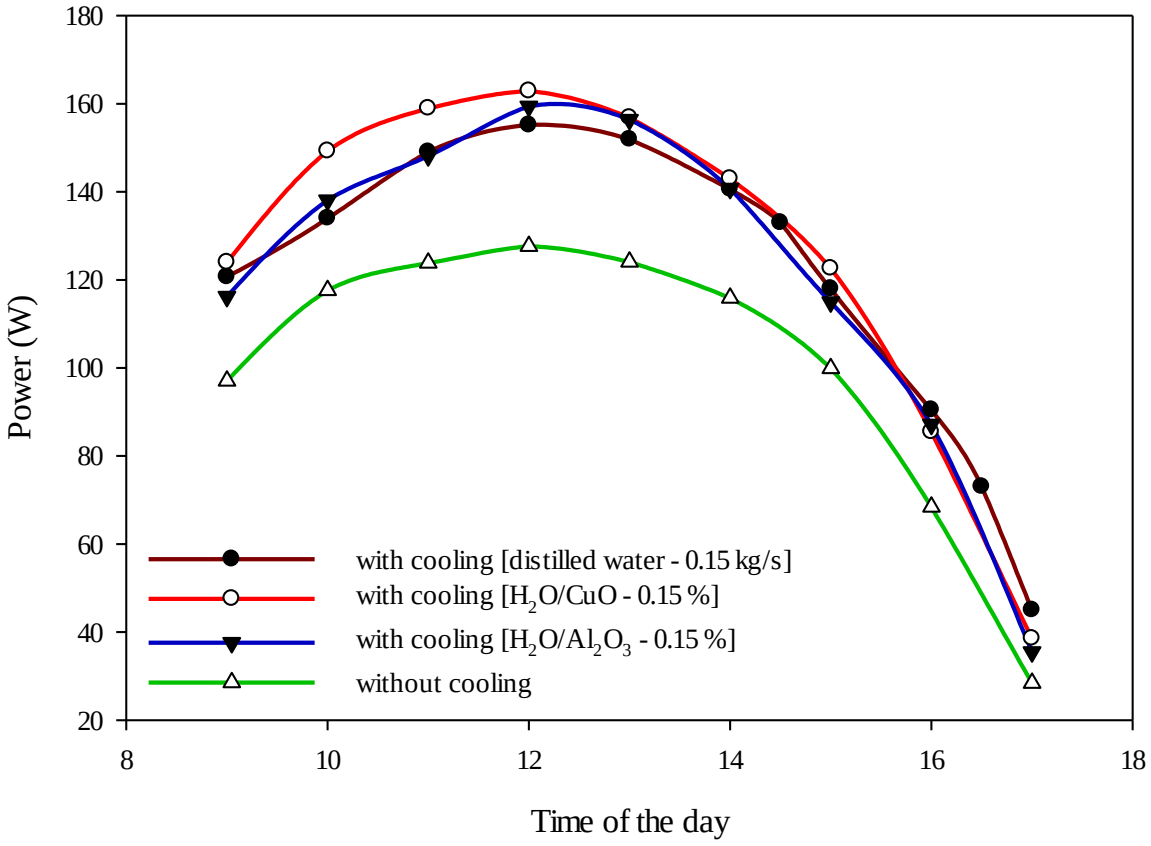

Fig. 23. Comparison between the power generated from the PV for different cooling fluids when design (2) was tested at optimal operating conditions.

3.1.3 Comparisons between Design (1) and Design (2)

Comparison between design (1) and (2) based on the PV-generated power is illustrated in Fig. 24 when distilled water was used as a coolant fluid. The superiority of design (1) can be seen in Fig 24 as the improvement in generated power reached to 5.77% compared to design 2 when distilled water was used for cooling. The improvement in generated power is also 28.5 % compared to that obtained by uncooled PV. Figure 24 shows that the maximum generated power was 162.445 W recorded at 12:00 pm when the PV was integrated with design (1) compared to 155.17 W for design

(2) when $\dot{m}_{HTF}$= 0.15 kg/s was used. The maximum generated power significantly improved to reach 178.1 W when design (1) was tested with CuO nano-fluid compared to 162.89 W for design (2) as shown in Fig. 25. Design (1) shows also better performance compared to design (2) when Al_2O_3 nano-fluid was used, as shown in Fig. 26. Up to 10 % and 37.49% more generated power was achieved when this design was used compared to design (2) and uncooled PV, respectively. The improvements in generated power achieved by design (1) can be seen in Figs. 24, 25, and 26, especially during the period from 9:00 am to 3:00 pm. During this period, high solar radiation was measured (960-1000 W/m^2) that causes a significant rise in PV surface temperature; therefore, the effect of the cooling was considerable and meaningful. After 3:00 no differences between the cooling designs from one side and the uncooled system from the other side due to the low recorded values of solar radiation and PV surface temperature. So, the effect of cooling is not noticeable after 3:00 pm.

Based on the above results, the PV with cooling design (1) achieves the better performance compared to design (2) at all studied cooling fluids.

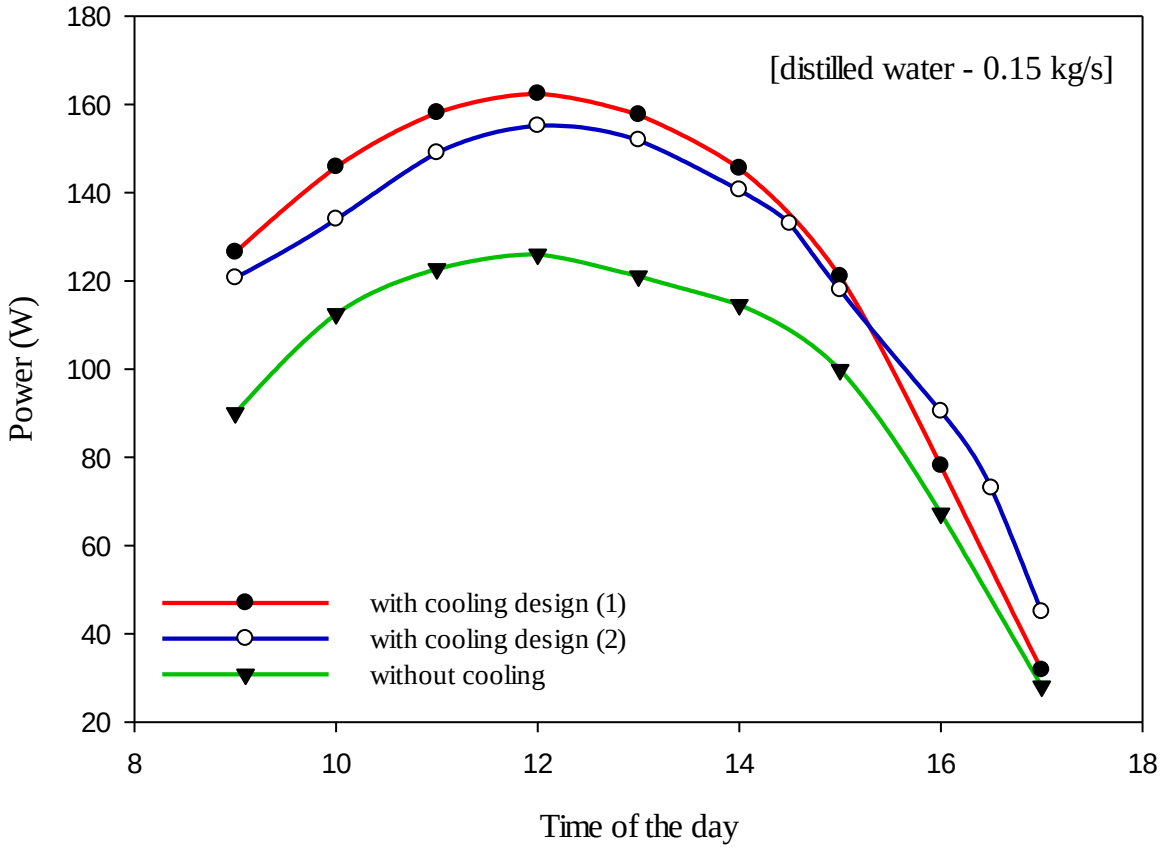

Fig. 24. Comparison between design (1) and (2) when distilled water was used as cooling fluid at $\dot{m}_{HTF}$= 0.15 kg/s.

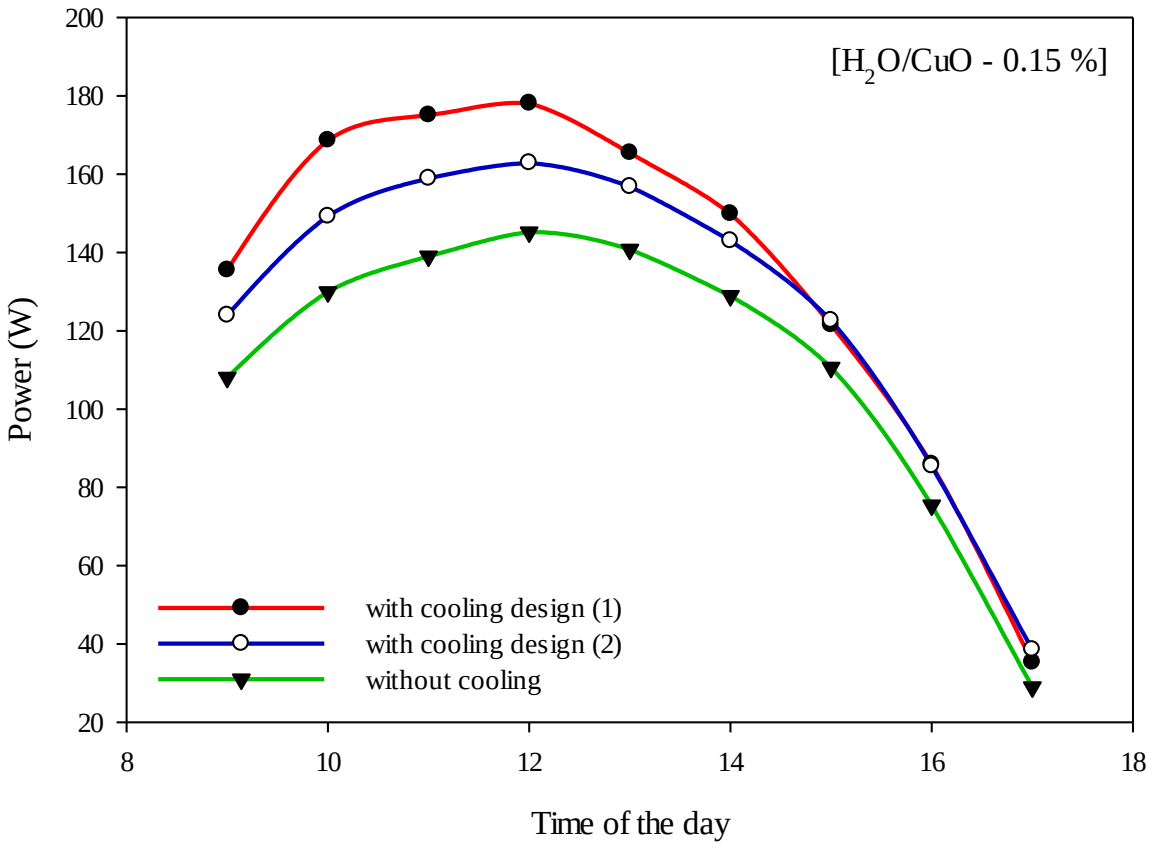

Fig. 25. Comparison between designs (1) and (2) when H_2O/CuO nano-fluid at concentration 0.15% was used as cooling fluid.

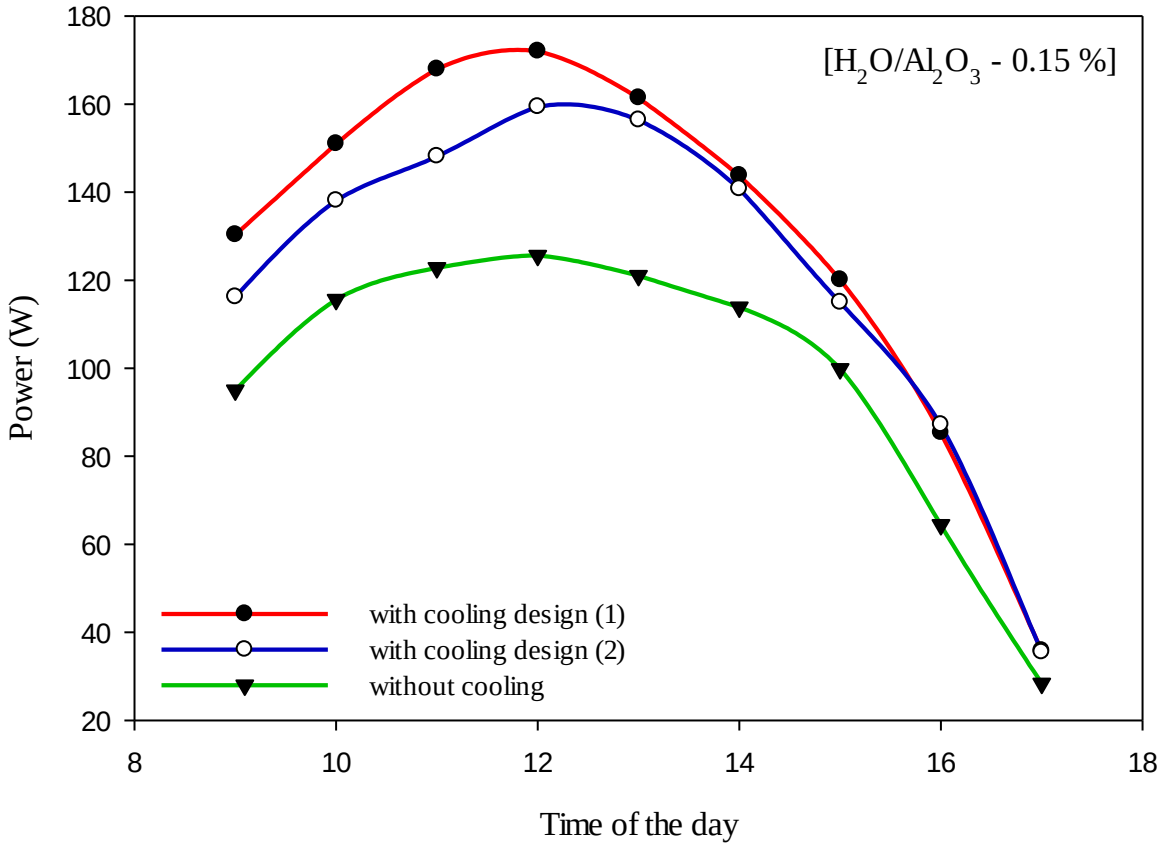

Fig. 26. Comparison between designs (1) and (2) when H_2O/Al_2O_3 nano-fluid at concentration 0.15% was used as cooling fluid.

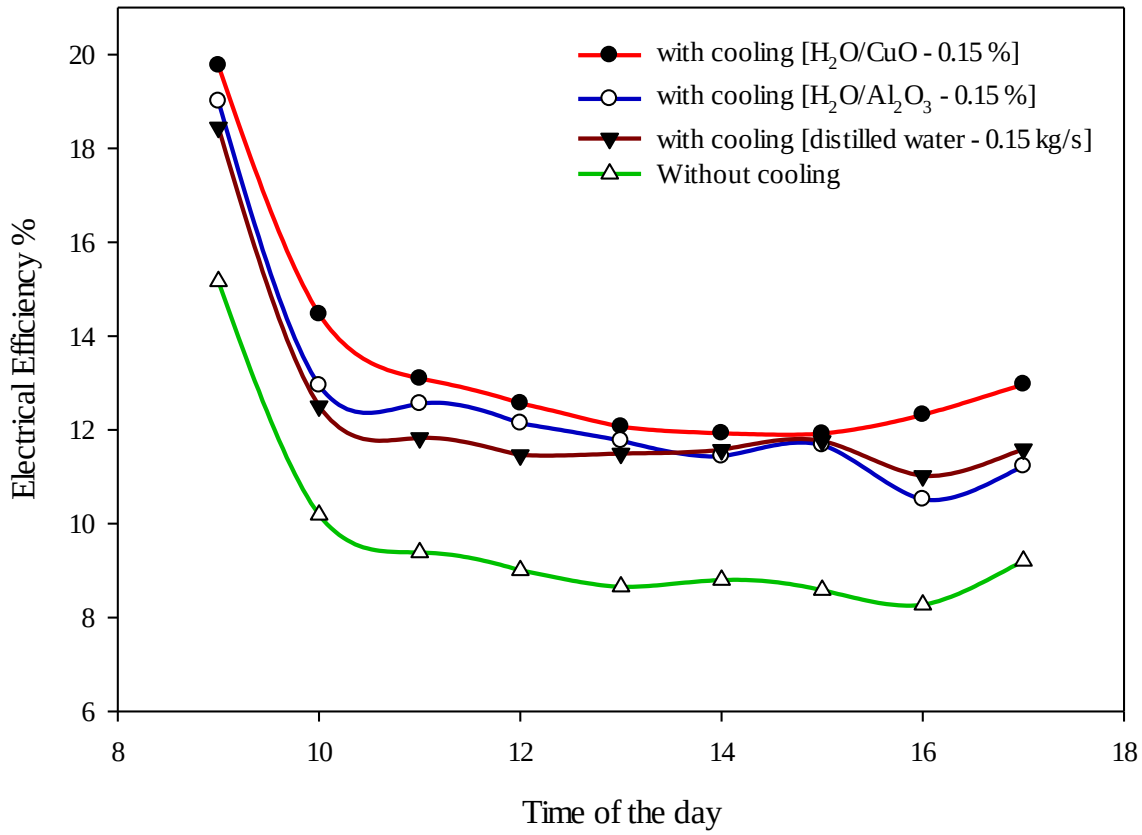

Fig. 27. Comparison between the efficiencies of design (1) only at different cooling fluids (CuO, Al_2O_3, distilled water) at optimal operating conditions**.**

For only design (1) cooling system, Fig. 27 compares the electrical efficiencies of the PV using different cooling fluids at optimal conditions. It can be clearly seen that using CuO nano-fluids at 0.15 % concentration gives the best PV electrical efficiency among the tested cooling fluids (distilled water and Al_2O_3 nano-fluid). The improvements in the PV electric efficiency reached 39.5, 34.8, and 27.3 % when CuO and Al_2O_3 nano-fluids and distilled water were used as cooling fluid, respectively, compared to the uncooled PV. The previously obtained results are close to that reported in the literature when nano-fluids were used for cooling the PV [23, 34, 35].

3.2 PV- RO desalination system

Based on the results displayed in section 3. 1, the cooling design (1) achieves the best performance of the PV when CuO nano-fluid of weight concentration of 0.15% was used at flow rate of 0.15 kg/s. So, the RO desalination plant was tested during the daylong when it was powered by the PV integrated with design (1). The experimental results showed that The PV integrated with the cooling design (1) is capable of providing the required power of the proposed RO system for 6 hrs/day. The effect of preheating the feed water of different salinities (1000, 2000, and 3000 mg L^{-1}) on the productivity of the desalination system was also studied. Indeed, the temperature control is very complicated in this case due to the feed water preheating based only on the heat recovery from the PV cooling system. This recovered heat is capable of increasing the feed water temperature from 30 to 36 ˚C during the working period from 9:00 am to 11:00 am. Then the temperature of feed water maintains approximately constant (36±0.5 ˚C) during the period from 11:00 to 2:00 pm. After that it gradually decreases to reach 34 ˚C at the end of working time (3:00 pm). So, the system was tested on successive days of September (14-19/09/2021) at different water salinities during the period from 12:00 pm to 1:00 pm to ensure that the feed water temperature is maintained constant at 36±0.5 ˚C. While the other temperature value (30 ˚C) is obtained when the feed water was used without preheating. So, two feed water temperatures are only considered: 30 ˚C (without preheating) and 36±0.5 ˚C (with preheating). During these experiments, the recorded solar radiation was found in the range from 960 to 986 W/m^2, the RO operating pressure was 8 bar, and the inlet pressure was 1.5 bar. As it is expected, the permeate flow decreases when the feed water salinity increases as can be seen in Table 3. Where the RO productivity was found 88.5, 68.5, and 54.8 L/h corresponding to 1000, 2000, and 3000 mg L^{-1} of the feed water salinity, respectively, when the system was tested without preheating. These productivities increased to 92,

72.9, 61 L/h, respectively, when the feed water was preheated to 36 ˚C. The previous result was expected because of the decreasing feed water viscosity and increasing permeation rate with the increase in feed water temperature. However, every membrane has an optimum temperature for best performance. This is due to the fact that separation efficiency decreases at temperatures above 35 ˚C because of increase in the diffusion coefficient and solute solubility. The results of Table 3 also shows that the highest increment in productivity due to the feed water preheating was achieved at salinity (3000 mg L^{-1}). This explains the importance of feed water preheating when high salinities are considered. The tests also showed that as the temperature of the feed water increase, the salinity of the productivity also increases. Therefore, it gives a negative effect on the product. This may be because increasing the feed water temperature decreases the water viscosity, and the membrane structure permits to water and salts as to pass through membranes easily [36]. The recovery factor is defined as the ratio of permeate flow rate to the feed water flow rate [26]. In all cases of feed water temperatures and salinities, the recovery factor of the RO system was calculated. It is found that when the feed water temperature increases, the recovery factor also increases. This is because higher diffusivity of the water leads to an increase in the water influx through the membrane, so a decrease in salt rejection was achieved. It was noticed that at 3000 mg L^{-1}, there is a higher recovery factor when the feed water temperature increased compared to other concentrations. This may be due to the amount of salt that transmitted through the membrane at this concentration, and this explanation is consistent with other studies [37-39]. For the purpose of comparison, the RO powered by PV with cooling design (2) and free of cooling were also tested. Science the same RO pilot plant is used in all tests, the plant gives the same productivity when the PV generated power is enough to power the proposed desalination system. The results showed that the PV is capable of driving the RO desalination system for 6 hrs/day (9:00 am- 3:00 pm) when

the cooling is implemented whatever the cooling design is. While, it drives the RO plant for only 4 hrs/day (10:00 am- 2:00 pm) when the uncooled PV was used.

Table 3. The results of the RO unit tests at different salt concentrations and two temperatures

	Feed water		Permeate		Brine		
	Flow rate (L/h)	TDS (mg L^{-1})	Flow rate (L/h)	TDS (mg L^{-1})	Flow rate (L/h)	TDS (mg L^{-1})	Recovery factor
30 ˚C	151.5	1000	88.5	45	63	2341.53	0.58
	151.5	2000	68.5	97	83	3570.53	0.45
	151.5	3000	54.8	250	96.7	4558.41	0.36
36±0.5 ˚C	151.5	1000	92	55	59.5	2461.15	0.61
	151.5	2000	72.9	130	78.6	3734.37	0.48
	151.5	3000	61	300	90.5	4819.87	0.40

3.2.1 Economic analysis

Economic analysis for the proposed PV-RO desalination plant was conducted based on the methodology introduced by Papapetrou et al. [40]. The total capital cost of a battery-less PV-RO system was calculated from the summation of capital cost for each component: PV module, cooling system, RO unit, and pump. It is assumed that 15% of the components cost is considered the installation cost of these components [41]. The lifetime of the PV module is considered 20 years, and RO was about 5 years. Since the lifetime of RO is only a quarter of the PV, four RO units are considered to be used during the lifetime of the system. Therefore, the capital cost of the PV (CC_{PV}) , RO (CC_{RO}), Pumps (CC_P), storage tank (CC_{st}) and cooling design (CC_{cd}) are calculated by the following Equations [41]:

$$CC_{PV}=1.15\times TP_{PV}, \quad (1)$$

$$CC_{RO}=1.15\times TP_{RO}, \quad (2)$$

$CC_P = 1.15 \times TP_P$, (3)

$CC_{st} = 1.15 \times TP_{st}$, (4)

$CC_{cd} = 1.15 \times TP_{cd}$. (5)

Where TP_{PV}, TP_{RO}, TP_P, TP_{st}, and TP_{cd}.are the total price of the PV module, RO unit, the used Pumps, storage tank and the cooling design, respectively. The prices of the different components are given in Table 4. The total capital cost (CC_{Total}) was calculated by Eq. (6).

$CC_{total} = CC_{RO} + CC_{PV} + CC_P + CC_{st} + CC_{cd}$. (6)

A simplified cost of water (SCOW) method was adopted [40] to estimate the water cost. This method uses the amortization factor because the bank or investor assumed the capital cost. The amortization factor was needed to annualize the total capital cost considering the interest rate and plant lifetime assumed to be 10% and 20 years, respectively. The annual operation and maintenance costs are also considered in this method, which was assumed 4% of the total capital cost [40]. The cost per meter square of fresh ($\boldsymbol{C_w}$) is calculated by using Eqs. (7) and (8) [40]:

$$\alpha = \frac{i*(1+i)^n}{(1+i)^n-1} \quad (7)$$

$$C_w = \frac{(CC_{total}*\alpha)+C_{ann}}{\sum W_p} \quad (8)$$

Where $\boldsymbol{\alpha}$ is the amortization factor, $\boldsymbol{C_{ann}}$ is the annual operation and maintenance cost, $\boldsymbol{\Sigma W_P}$ is the annual water production, $\boldsymbol{i}$ is the interest rate, and $\boldsymbol{n}$ is the plant lifetime. As expected the C_w increases when the salinity of water increases in all studied cases as seen in Table 5. The feed water preheating has a significant positive effects on the C_w especially when cooling design (2) was used. The calculated results also showed that the PV integrated with cooling design (1)

operated at the optimal condition achieves the lowest $\boldsymbol{C_w}$ (0.74-1.12 \$/m^3) when the preheating technique was implemented. It also achieves lower cost even the preheating was not applied compared to design (2) and the PV without cooling as clearly seen in Table 5. It is also noticed that lower values of C_w of 0.97-1.58 \$/m^3 were obtained when the PV without cooling was used compared to 1.02-1.65 \$/m^3 for design (2) without preheating the feed water. While, the PV integrated with design (2) achieves lower values of C_w when the preheating is implemented at water salinities higher than or equal 2000 ppm compared to the uncooled system as shown in Table 5. The high values of C_w associated with design (2) explain the importance of selecting the cooling system material and the compromisation between its thermal properties and cost. Where, the channels and the flat plate used in this design is made of copper that has high thermal conductivity and relatively high cost. Based on the previous results, it is recommended to use the PV integrated with design (1) to power the RO when the feed water preheating is implemented. In this case, the C_w was found in the range 0.74-1.12 \$/m^3. This cost is considered very low compared to 3.1 \$/m^3 [42] when uncooled PV integrated with batteries was used to drive the RO at water salinity 2000 ppm. it is also low compared to 1.41 \$/m^3 [43] when a battery-less PV without cooling was used to drive the RO at water salinity 3500 ppm. The proposed PV-RO without cooling has also competitive costs of 1.26 and 1.58 \$/m^3 at water salinities 2000 and 3000, respectively, compared to the uncooled PV-RO [42, 43].

Table 4. The total price of the different components of the proposed system.

The component	The total price (\$)
RO unit	321
PV module	225
High pressure Pump	32
Circulating pump	22.5
Cooling design 1	65

Cooling design 2	310
Saline water storage tank	92.5

Table 5. The cost per meter square of fresh water produced from PV-RO for the two cooling designs when CuO nano-fluid was used as cooling fluid.

	Design (1)				**Design (2)**			**Without cooling**	
	TDS (ppm)	Permeate flow rate (L/h)	Daily productivity (L)	Cost ($/m^3)	Permeate flow rate (L/h)	Daily productivity (L)	Cost ($/m^3)	Daily productivity (L)	Cost ($/m^3)
30 ˚C	1000	**88.5**	**531**	**0.77**	88.5	531	1.02	354	0.97
	2000	**68.5**	**411**	**0.99**	68.5	411	1.32	274	1.26
	3000	**54.8**	**328.8**	**1.24**	54.8	328.8	1.65	219.2	1.58
36±0.5 ˚C	1000	**92**	**552**	**0.74**	92	552	0.98	-	
	2000	**72.9**	**437.4**	**0.93**	72.9	437.4	1.24		
	3000	**61**	**366**	**1.12**	61	366	1.49		

4. Conclusions

In this work, two PV cooling designs was tested at different flow rate of HTF. Two types of nano-fluid, namely CuO and Al_2O_3 with distilled water as base fluid, were also tested as cooling fluid. Based on the obtained experimental results, the following conclusions were extracted:

- The PV performance was significantly improved when the cooling technique was implemented, whatever the proposed cooling design, and cooling fluid were.
- The optimal cooling flow rate in the two designs was found 0.15 kg/s.
- Better performance was achieved when design (1) was used to cool the PV compared to design (2) at all tested cooling fluids.
- When the weight concentration of nano-fluid increases, the PV surface temperature decreases, and the efficiency and generated power increases for the two studied nano-fluids.
- The results also showed a superiority of copper oxide nano-fluid compared to aluminum oxide nano-fluid in the two cooling designs.
- The improvements in the electric efficiency of the PV integrated with design (1) reached 39.5, 34.8 and 27.3 % when CuO and Al_2O_3 nano-fluids and distilled water were used as cooling fluid, respectively, compared to the uncooled PV.
- The PV integrated with cooling design (1) can be operated for 6 hrs/day with sufficient power to drive the RO plant when the CuO nano-fluid was used as cooling fluid at the optimal operation parameter.
- The necessary of preheating the feed water was plainly observed especially at high water salinities.

- The proposed PV-RO desalination system showed high commercialization potential as it achieves very low cost of fresh water production.

References

[1] S. Shalaby, E. El-Bialy, and A. El-Sebaii, "An experimental investigation of a v-corrugated absorber single-basin solar still using PCM," *Desalination,* vol. 398, pp. 247-255, 2016.

[2] S. M. Shalaby, A. E. Kabeel, B. M. Moharram, and A. H. Fleafl, "Experimental study of hybrid solar humidification dehumidification system for extremely saline water desalination," *Energy Conversion and Management,* vol. 235, p. 114021, 2021/05/01/ 2021, doi: https://doi.org/10.1016/j.enconman.2021.114021.

[3] M. Abdelgaied *et al.*, "Performance assessment of solar PV-driven hybrid HDH-RO desalination system integrated with energy recovery units and solar collectors: Theoretical approach," *Energy Conversion and Management,* vol. 239, p. 114215, 2021/07/01/ 2021, doi: https://doi.org/10.1016/j.enconman.2021.114215.

[4] W. D. Childs, A. E. Dabiri, H. A. Al-Hinai, and H. A. Abdullah, "VARI-RO solar-powered desalting technology," *Desalination,* vol. 125, no. 1-3, pp. 155-166, 1999.

[5] S. M. Shalaby, "Reverse osmosis desalination powered by photovoltaic and solar Rankine cycle power systems: A review," *Renewable and Sustainable Energy Reviews,* vol. 73, pp. 789-797, 2017/06/01/ 2017, doi: https://doi.org/10.1016/j.rser.2017.01.170.

[6] D. Manolakos, E. S. Mohamed, I. Karagiannis, and G. Papadakis, "Technical and economic comparison between PV-RO system and RO-Solar Rankine system. Case study: Thirasia island," *Desalination,* vol. 221, no. 1, pp. 37-46, 2008/03/01/ 2008, doi: https://doi.org/10.1016/j.desal.2007.01.066.

[7] E. S. Mohamed, G. Papadakis, E. Mathioulakis, and V. Belessiotis, "A direct coupled photovoltaic seawater reverse osmosis desalination system toward battery based systems — a technical and economical experimental comparative study," *Desalination,* vol. 221, no. 1, pp. 17-22, 2008/03/01/ 2008, doi: https://doi.org/10.1016/j.desal.2007.01.065.

[8] H. Vyas *et al.*, "Modus operandi for maximizing energy efficiency and increasing permeate flux of community scale solar powered reverse osmosis systems," *Energy Conversion and Management,* vol. 103, pp. 94-103, 2015/10/01/ 2015, doi: https://doi.org/10.1016/j.enconman.2015.05.076.

[9] A. Soric, R. Cesaro, P. Perez, E. Guiol, and P. Moulin, "Eausmose project desalination by reverse osmosis and batteryless solar energy: Design for a 1m3 per day delivery," *Desalination,* vol. 301, pp. 67-74, 2012/09/03/ 2012, doi: https://doi.org/10.1016/j.desal.2012.06.013.

[10] L. C. Kelley and S. Dubowsky, "Thermal control to maximize photovoltaic powered reverse osmosis desalination systems productivity," *Desalination,* vol. 314, pp. 10-19, 2013/04/02/ 2013, doi: https://doi.org/10.1016/j.desal.2012.11.036.

[11] T. A. Ajiwiguna, G.-R. Lee, B.-J. Lim, S.-M. Choi, and C.-D. Park, "Design strategy and economic analysis on various configurations of stand-alone PV-RO systems," *Desalination,* vol. 526, p. 115547, 2022/03/15/ 2022, doi: https://doi.org/10.1016/j.desal.2022.115547.

[12] J. Tonui and Y. Tripanagnostopoulos, "Improved PV/T solar collectors with heat extraction by forced or natural air circulation," *Renewable energy,* vol. 32, no. 4, pp. 623-637, 2007.
[13] M. R. Gomaa, W. Hammad, M. Al-Dhaifallah, and H. Rezk, "Performance enhancement of grid-tied PV system through proposed design cooling techniques: An experimental study and comparative analysis," *Solar Energy,* vol. 211, pp. 1110-1127, 2020.
[14] S. Krauter, "Increased electrical yield via water flow over the front of photovoltaic panels," *Solar Energy Materials and Solar Cells,* vol. 82, no. 1, pp. 131-137, 2004/05/01/ 2004, doi: https://doi.org/10.1016/j.solmat.2004.01.011.
[15] S. Odeh and M. Behnia, "Improving photovoltaic module efficiency using water cooling," *Heat Transfer Engineering,* vol. 30, no. 6, pp. 499-505, 2009.
[16] A. Royne and C. J. Dey, "Design of a jet impingement cooling device for densely packed PV cells under high concentration," *Solar energy,* vol. 81, no. 8, pp. 1014-1024, 2007.
[17] M. Abdolzadeh and M. Ameri, "Improving the effectiveness of a photovoltaic water pumping system by spraying water over the front of photovoltaic cells," *Renewable Energy,* vol. 34, no. 1, pp. 91-96, 2009/01/01/ 2009, doi: https://doi.org/10.1016/j.renene.2008.03.024.
[18] S. Nižetić, D. Čoko, A. Yadav, and F. Grubišić-Čabo, "Water spray cooling technique applied on a photovoltaic panel: The performance response," *Energy Conversion and Management,* vol. 108, pp. 287-296, 2016/01/15/ 2016, doi: https://doi.org/10.1016/j.enconman.2015.10.079.
[19] M. Mohsenzadeh and R. Hosseini, "A photovoltaic/thermal system with a combination of a booster diffuse reflector and vacuum tube for generation of electricity and hot water production," *Renewable Energy,* vol. 78, pp. 245-252, 2015/06/01/ 2015, doi: https://doi.org/10.1016/j.renene.2015.01.010.
[20] P. Prudhvi and P. C. Sai, "Efficiency improvement of solar PV panels using active cooling," in *2012 11th International Conference on Environment and Electrical Engineering*, 18-25 May 2012 2012, pp. 1093-1097, doi: 10.1109/EEEIC.2012.6221543.
[21] M. Chandrasekar, S. Suresh, T. Senthilkumar, and M. Ganesh karthikeyan, "Passive cooling of standalone flat PV module with cotton wick structures," *Energy Conversion and Management,* vol. 71, pp. 43-50, 2013/07/01/ 2013, doi: https://doi.org/10.1016/j.enconman.2013.03.012.
[22] M. Ghadiri, M. Sardarabadi, M. Pasandideh-fard, and A. J. Moghadam, "Experimental investigation of a PVT system performance using nano ferrofluids," *Energy Conversion and Management,* vol. 103, pp. 468-476, 2015.
[23] M. S. Ebaid, A. M. Ghrair, and M. Al-Busoul, "Experimental investigation of cooling photovoltaic (PV) panels using (TiO2) nanofluid in water-polyethylene glycol mixture and (Al2O3) nanofluid in water-cetyltrimethylammonium bromide mixture," *Energy Conversion and Management,* vol. 155, pp. 324-343, 2018.
[24] A. A. Monjezi *et al.*, "Development of an off-grid solar energy powered reverse osmosis desalination system for continuous production of freshwater with integrated photovoltaic thermal (PVT) cooling," *Desalination,* vol. 495, p. 114679, 2020/12/01/ 2020, doi: https://doi.org/10.1016/j.desal.2020.114679.
[25] S. Gorjian, B. Ghobadian, F. J. Jamshidian, H. Sharon, and S. Saadi, "Performance evaluation and economics of a locally-made stand-alone hybrid photovoltaic-thermal

brackish water reverse osmosis unit," *Cleaner Engineering and Technology*, vol. 2, p. 100078, 2021/06/01/ 2021, doi: https://doi.org/10.1016/j.clet.2021.100078.
[26] R. Talebnejad *et al.*, "A new cooling method for photovoltaic panels using brine from reverse osmosis units to increase efficiency and improve productivity," *Energy Conversion and Management*, vol. 251, p. 115031, 2022/01/01/ 2022, doi: https://doi.org/10.1016/j.enconman.2021.115031.
[27] S. M. Shalaby, A. E. Kabeel, B. M. Moharram, and A. H. Fleafl, "Experimental study of the solar water heater integrated with shell and finned tube latent heat storage system," *Journal of Energy Storage*, vol. 31, p. 101628, 2020/10/01/ 2020, doi: https://doi.org/10.1016/j.est.2020.101628.
[28] M. H. Nia *et al.*, "Stabilizing and dispersing methods of TiO2 nanoparticles in biological studies," *Archives of Advances in Biosciences*, vol. 6, no. 2, pp. 96-105, 2015.
[29] W. Pang, Y. Cui, Q. Zhang, H. Yu, L. Zhang, and H. Yan, "Experimental effect of high mass flow rate and volume cooling on performance of a water-type PV/T collector," *Solar Energy*, vol. 188, pp. 1360-1368, 2019.
[30] M. Hossain, A. Pandey, J. Selvaraj, N. Abd Rahim, A. Rivai, and V. Tyagi, "Thermal performance analysis of parallel serpentine flow based photovoltaic/thermal (PV/T) system under composite climate of Malaysia," *Applied Thermal Engineering*, vol. 153, pp. 861-871, 2019.
[31] S. Shalaby, M. Elfakharany, B. Moharram, and H. Abosheiasha, "Experimental study on the performance of PV with water cooling," *Energy Reports*, vol. 8, pp. 957-961, 2022.
[32] A. H. Al-Waeli *et al.*, "Evaluation of the nanofluid and nano-PCM based photovoltaic thermal (PVT) system: An experimental study," *Energy Conversion and Management*, vol. 151, pp. 693-708, 2017.
[33] X. Yang, L. Sun, Y. Yuan, X. Zhao, and X. Cao, "Experimental investigation on performance comparison of PV/T-PCM system and PV/T system," *Renewable energy*, vol. 119, pp. 152-159, 2018.
[34] S. R. Abdallah, I. M. Elsemary, A. A. Altohamy, M. Abdelrahman, A. A. Attia, and O. E. Abdellatif, "Experimental investigation on the effect of using nano fluid (Al2O3-Water) on the performance of PV/T system," *Thermal Science and Engineering Progress*, vol. 7, pp. 1-7, 2018.
[35] A. N. Al-Shamani, K. Sopian, S. Mat, H. A. Hasan, A. M. Abed, and M. Ruslan, "Experimental studies of rectangular tube absorber photovoltaic thermal collector with various types of nanofluids under the tropical climate conditions," *Energy Conversion and Management*, vol. 124, pp. 528-542, 2016.
[36] M. Wilf and K. Klinko, "Optimization of seawater RO systems design," *Desalination*, vol. 138, no. 1-3, pp. 299-306, 2001.
[37] S. A. Mohammed, A. D. Abbas, and L. S. Sabry, "Effect of operating conditions on reverse osmosis (RO) membrane performance," *J Eng*, vol. 20, pp. 61-70, 2014.
[38] M. S. Atab, A. Smallbone, and A. Roskilly, "An operational and economic study of a reverse osmosis desalination system for potable water and land irrigation," *Desalination*, vol. 397, pp. 174-184, 2016.
[39] X. Jin, A. Jawor, S. Kim, and E. M. Hoek, "Effects of feed water temperature on separation performance and organic fouling of brackish water RO membranes," *Desalination*, vol. 239, no. 1-3, pp. 346-359, 2009.

[40] M. Papapetrou, A. Cipollina, U. La Commare, G. Micale, G. Zaragoza, and G. Kosmadakis, "Assessment of methodologies and data used to calculate desalination costs," *Desalination*, vol. 419, pp. 8-19, 2017.
[41] E. S. Mohamed and G. Papadakis, "Design, simulation and economic analysis of a stand-alone reverse osmosis desalination unit powered by wind turbines and photovoltaics," *Desalination*, vol. 164, no. 1, pp. 87-97, 2004/03/25/ 2004, doi: https://doi.org/10.1016/S0011-9164(04)00159-6.
[42] M. A. Alghoul *et al.*, "Design and experimental performance of brackish water reverse osmosis desalination unit powered by 2 kW photovoltaic system," *Renewable Energy*, vol. 93, pp. 101-114, 2016/08/01/ 2016, doi: https://doi.org/10.1016/j.renene.2016.02.015.
[43] G. D. Pimentel da Silva and M. H. Sharqawy, "Techno-economic analysis of low impact solar brackish water desalination system in the Brazilian Semiarid region," *Journal of Cleaner Production*, vol. 248, p. 119255, 2020/03/01/ 2020, doi: https://doi.org/10.1016/j.jclepro.2019.119255.